

Evidence of orbital mixing upon ionization via Cooper minimum photoelectron dynamics in epichlorohydrin. Experiment and Theory.

L. Schio,^{1,2} M. Alagia,¹ T. Moitra,^{3,4} D. Toffoli,⁵ A. Ponzi,⁶ M. Stener,⁵ S. Coriani,³ P. Decleva,^{5, a)} O. Rebrov,⁷ V. Zhaunerchyk,⁸ M. Larsson,⁷ S. Falcinelli,⁹ A. A. Dias,¹⁰ D. Catone,¹¹ S. Turchini,¹¹ N. Zema,¹¹ F. Salvador,¹¹ D. Benedetti,¹ D. Vivoda,¹² B. Botta,¹³ and S. Stranges^{13, 1, b)}

¹⁾ *CNR - Istituto Officina dei Materiali (IOM), Laboratorio TASC, Area Science Park Basovizza, Trieste, Italy*

²⁾ *Department of Basic and Applied Science for Engineering (SBAI), Sapienza University, Rome, Italy*

³⁾ *DTU Chemistry, Technical University of Denmark, Kemitorvet 207, 2800 Kongens Lyngby, Denmark*

⁴⁾ *Department of Physical and Theoretical Chemistry, Faculty of Natural Sciences, Comenius University, SK-84215, Bratislava, Slovakia*

⁵⁾ *Dipartimento di Scienze Chimiche e Farmaceutiche, Università degli Studi di Trieste, Trieste, Italy*

⁶⁾ *Institut Ruder Bošković, Bijeniška cesta 54, 10000 Zagreb, Croatia*

⁷⁾ *Department of Physics, University of Stockholm, Stockholm, Sweden*

⁸⁾ *Department of Physics, University of Gothenburg, Gothenburg, Sweden*

⁹⁾ *Dipartimento di Ingegneria Civile ed Ambientale, Università degli Studi di Perugia, Perugia, Italy*

¹⁰⁾ *Laboratory for Instrumentation, Biomedical Engineering, and Radiation Physics, Departamento de Física, Faculdade de Ciências e Tecnologia, Universidade NOVA de Lisboa, Capacarica, Portugal*

¹¹⁾ *CNR-ISM, Area della Ricerca di Roma Tor Vergata, Via del Fosso del Cavaliere 100, Roma, Italy*

¹²⁾ *Elettra-Sincrotrone Trieste, Area Science Park, Basovizza, Trieste, Italy*

¹³⁾ *Department of Chemistry and Technologies of Drugs, Sapienza University, I-00183, Rome, Italy*

(Dated: 27 February 2026)

A peculiar electron correlation effect, leading to orbital rotation upon ionization, theoretically predicted long ago, was never experimentally characterized. The effect is expected to appear prominently in the photoionization of chiral molecules, due to the lack of symmetry constraints to wave-functions mixing. This is observed to have a profound effect on the photoelectron dynamics, as here demonstrated by investigating β asymmetry parameters and partial cross-section observables in the Cl 3p Cooper minimum region of epichlorohydrin, a chiral prototype system.

Angle-resolved photoelectron spectroscopy with tunable synchrotron radiation allowed measuring Cooper minimum β oscillations, which were observed for solely two valence photoionization channels. The nature and number of channels exhibiting such dynamical behavior, along with the extent of the observed oscillation amplitudes, could not be accounted for by predictions based on Hartree-Fock (HF) and Density Functional Theory (DFT). These features could only be explained by incorporating correlation effects, which mix single-hole configurations of identical symmetry, in the characterization of the four lowest-lying molecular cation states, via equation-of-motion coupled cluster singles and doubles Dyson orbitals.

I. INTRODUCTION

Removal of a single electron (for instance, by photoionization) is the most elementary excitation of a many-body system. In the Independent Particle Approximation (IPA), it is directly connected with the negative orbital energies, and photoionization has provided an enormous understanding of the orbital structure of molecules. However, the IPA is only a first-order model and thus offers only a simplified representation of electron inter-

actions. Correlation effects alter this picture in several ways, so photoionization offers a unique laboratory to study correlation effects. Indeed, a strong interplay between photoionization experiments and electronic structure theory has existed since the inception of the technique.¹⁻³

Among the several effects displayed and analyzed, one of the most elusive is *orbital mixing*, i.e., the fact that the “electron-hole” orbital relative to a particular final ionic state, instead of resembling one of the occupied Hartree-Fock (HF) orbitals of the ground state, is a linear combination, with significantly large coefficients, of two or more of them, but still of norm close to one. In more precise terms, the Dyson orbital,⁴⁻⁷ which characterizes ionization to a specific final state, becomes a mixture of

^{a)} Electronic mail: decleva@units.it

^{b)} Electronic mail: stefano.stranges@uniroma1.it

ground-state orbitals and can be considered as a kind of orbital rotation upon ionization.

Although discovered theoretically many years ago,^{8,9} orbital mixing has remained (until now) a theoretical curiosity, since it cannot be assessed on pure energy grounds—that is, by means of photoelectron spectroscopy. Specifically, it is well established that electron-correlation effects in inner-valence molecular ionization lead to a breakdown of the independent-electron approximation, giving rise to shake-up and shake-down processes. Experimentally, these are readily observed as satellite transitions at energies displaced from the main line. However, with the advent of more advanced computational methods, it has become clear that weaker correlation effects can also mix canonical orbitals in the outer-valence region, where the independent-electron picture has traditionally been assumed to hold. A challenge for experimental verification is that such mixing only minimally perturbs the eigenvalues, causing any shifts in ionization energies to remain essentially undetectable. Only transition properties, typically dynamical photoionization observables like cross sections or angular distributions, can probe the nature of the Dyson orbital and reveal differences in its composition. This effect is characteristic of the outer valence shell, where electron correlation is generally weaker, hence not to the point of complete breakdown of the single-particle picture, as is commonly observed in the inner valence region.^{10,11} It may be associated with differential relaxation properties of the HF orbitals, e.g., due to different localization/delocalization structure, or differential correlation of their main atomic orbital (AO) composition. This is often the case between s, p and d AO's in transition metal complexes,¹² and even between s, p orbitals relative to different shells, like in elements of the second and third period. Obviously, the mixing is easier when initial orbital energies are quite close, so that a relatively small perturbation can induce significant mixing. Thus, mixing is expected to be common in molecules with a dense manifold of outer valence orbitals of the same symmetry, which are the only ones allowed to mix. This is commonly the case in low-symmetry systems, and indeed orbital mixing may prove rather frequent in chiral molecules with no symmetry. A recent surge of interest in the phenomenon has been stimulated by the possibility of inducing the formation of a non-stationary electron wavepacket by photoionization and studying attosecond phenomena,⁹ for instance charge migration in pump-probe experiments, e.g. in propiolic acid¹³ and the PENNA molecule.¹⁴ An example has also been detected in studying photoelectron circular dichroism (PECD) in ionization of a chiral molecule.¹⁵ Photoelectron dynamics involves the study of properties of photoelectrons emitted from matter. In the case of randomly-oriented species and in the electric dipole approximation, it entails the knowledge of the partial, angle-integrated, photoionization cross sections (σ), and of the angular distribution (the β asymmetry or anisotropy parameter) as a function of photon energy.

Moreover, specific of chiral systems with circularly polarized light, a further angular (dichroic) parameter, β_1 or D , can be obtained, the so-called PECD effect. The experimental determination of these observables is ideally performed with synchrotron radiation (SR), an easily tunable photon source with controlled polarization, and Angle-Resolved PhotoElectron Spectroscopy (ARPES). One of the most striking and informative dynamical effects exhibited by $\sigma(h\nu)$ and $\beta(h\nu)$ is the Cooper minimum (CM).^{16,17} This phenomenon manifests itself in the form of a minimum of $\sigma(h\nu)$ when the photoionization process involves electron ejection from an atomic orbital with a radial node, since the minimum occurs because of the change in sign of radial matrix elements governing the transition moment, as the photon energy is increased from the ionization threshold. Concomitant with this σ behavior, the β parameter is strongly affected and displays, in the same CM energy region, a rapid oscillation characterized by a maximum and minimum. This latter, β_{\min} , occurs at a photon energy which approaches closely that of σ_{\min} . The CM phenomenon was thoroughly investigated theoretically^{16,17} and experimentally^{18–21} as a purely atomic effect. Interestingly, this effect was discovered to persist also in molecular photoionization by Carlson and co-workers.^{22–27} Minima in both σ and β were experimentally observed, and theoretically confirmed, for all cases in which the photoionization process, in the one-electron picture, involves the electron ejection from a non-bonding MO (lone-pair) with strong atomic character due to an AO with radial nodes, namely the S 3p or Cl 3p lone-pairs in the investigated systems. The good agreement between the measured and the calculated profiles of both σ and β allowed to associate the atomic CM phenomenon with a molecular CM. This concept was further enriched by observing CM dynamical effects, although of lesser extent, in photoionization processes involving σ -bonding MOs with partial contribution from AOs with radial nodes.^{22–29} Generally, the CM dynamical features of β are found to be much more pronounced than those of σ , making β the most sensitive probe with regard to CM dynamics. Such values are easier to measure experimentally than the corresponding σ value changes. It was found that the lower the β_{\min} value, the closer is the nature of the MO to the AO from which it derives, as revealed, for instance, by the Cl 3p AO contributions to different MOs involved in a large number of chlorinated molecules.^{22,24–30} Analogous studies were also accomplished on bromine atom CM in bromobenzene.^{31–33}

The characterization of orbital nature via detection of the CM offers a remarkable experimental possibility of detecting the orbital rotation effect. Because of the complexity and lack of symmetry of chiral molecules, with an associated manifold of closely lying ionic states, such effects can be expected to be quite common in such systems.

Monosubstituted oxiranes (ethylene oxides) have been studied experimentally and theoretically as important

model chiral molecules. Particularly, methyloxirane (C_3H_6O , also known as propylene oxide) has been studied with SR by several authors.^{34–37} The interaction of chiral molecules with circularly polarized radiation is considered to be a plausible mechanism connected to the abiotic origin of life. In this context, it is worth mentioning that propylene oxide has recently been detected in space as the first organic chiral molecule.³⁸ (Chloromethyl)oxirane (epichlorohydrin), derived from methyloxirane by hydrogen substitution with chlorine, has also been investigated with SR.^{39,40}

In the present work, we report very clear evidence of the phenomenon of orbital mixing in the asymmetry parameter β (and in the cross section σ) in the photoionization of epichlorohydrin, where the participation of Cl 3p AO's can be experimentally highlighted by the very strong Cooper minimum effect in the asymmetry parameters. A high-level theoretical treatment is provided, showing excellent agreement with the experimental results, indicating the interplay of correlation in the bound states, described by accurate Dyson orbitals obtained by the highly correlated equation-of-motion (EOM) coupled cluster singles and double (CCSD) approach,^{6,41–43} coupled with a time-dependent density functional theory (TDDFT) description of the molecular continuum, which includes interchannel coupling.^{43–45}

II. METHOD

A. Experimental

The experimental PE spectra were measured on the Circularly Polarized Beamline⁴⁶ of ELETTRA (Trieste), by photoionization of epichlorohydrin racemic samples (Aldrich, $\geq 99\%$ purity) with linearly polarized radiation. The PE spectra were recorded in the 13–54 eV photon energy range using the ARPES-TPES end station^{47–50} by operating the electron spectrometer in the ARPES mode. Both electron detection angles of 0° and 54.7° (the magic angle) with respect to the polarization plane of the linearly polarized radiation were set. The asymmetry parameters $\beta_i(h\nu)$, characterizing the photoelectron angular distribution, were measured as a function of photon energy as derived from the equation $\beta = (R - 1)$,^{51,52} with $R = A(0^\circ)/A(54.7^\circ)$ being the ratio between the peak areas of the considered PE band obtained at $\theta = 0^\circ$ and $\theta = 54.7^\circ$, respectively. The vapour, generated from the epichlorohydrin liquid sample, was admitted to the interaction region by an effusive source through a non-magnetic hypodermic needle. The liquid sample was kept at room temperature (23°C) during the measurements, and the gas rating was adjusted to set a constant pressure of 1.0×10^{-6} mbar in the ionization chamber. This pressure was monitored during the experiment. For signal normalization purpose, the incident photon flux was recorded, along with the photoelectron signal, with two different methods, namely as current of a silicon photo-

diode (IRD-AXUV-100) set as beam stopper after the interaction region, and as current of the gold-coated re-focusing mirror mounted at the entrance of the ionization chamber. The measurements, performed in a large photon energy range, required using both the Normal Incidence Monochromator (NIM) and the Spherical Grazing monochromator (SGM) of the beamline. The PE spectra were corrected by the spectrometer transmission function, as appropriate, considering the change in electron detection efficiency due to the different value of the electron kinetic energy and the selected constant-pass energy value. For this purpose, PE spectra of two reference gases, He and Ar, were recorded at the magic angle and at different kinetic energies and pass energies (5 eV and 10 eV). Furthermore, the PE spectrum of the first four PE bands of epichlorohydrin was systematically acquired at the photon energies 22.5 eV (NIM range) and 34.5 eV (SGM range) and at 0° detection angle, as reference spectra, to monitor possible small changes in the density of the vapour sample in the ionization region during the measurements.

The $\sigma_i(h\nu)$ and $\beta_i(h\nu)$ values were extracted from the spectra by determining the relative intensities of single PE components via a global multipeak fitting (see Section S1 for details). Spectra were first normalized to the photon flux and molecular target density, and corrected for the spectrometer transmission. Backgrounds, modeled as an arctan plus linear term, were obtained from spectra without epichlorohydrin using χ^2 fitting and subtracted, including the onset region. This correction was particularly important at low PE kinetic energies. All bands, being asymmetric with longer high-IE tails, were fit using asymmetric bi-Gaussian functions^{53,54} (two half-Gaussians sharing a peak maximum) described by four parameters: peak position (E_0), left and right widths (σ_l , σ_r), and scale factor δ , this latter being related to the peak area ($\delta(\sigma_l + \sigma_r)/2$) and the peak height ($\delta/\sqrt{2\pi}$). The first band (24a MO) position was treated as a free parameter per spectrum and aligned to Ref. 40, while other bands' positions were expressed relative to the HOMO and shared across spectra. For the first four bands, each peak retained individual shapes, whereas the six higher-energy bands shared a common shape (single σ_l and σ_r) across photon energies and angles. Scale factors δ_i were free for each spectrum. All spectra, measured at different photon energies for both $\theta = 0^\circ$ and $\theta = 54.7^\circ$ detection angles, were simultaneously fit in the global multipeak analysis.

This procedure provided a consistent measurement of the PE band relative intensities and enabled the extraction of $\beta_i(h\nu)$ and $\sigma_i(h\nu)$ for the valence photoionization channels of epichlorohydrin as a function of photon energy. Errors on the epichlorohydrin β values were estimated by measuring, with the same experimental procedure, well-known asymmetry parameters of reference gases, namely Ar, He and O_2 , in a wide photon energy range and exhibiting a large variety of β values.^{55–57}

B. Theoretical

The differential cross section for photoionization relative to a final ionic state Ψ_i^{N-1} (for randomly oriented molecules and linearly polarized light, in the dipole approximation) is given by the well known formula

$$\frac{d\sigma_i}{d\theta} = \frac{\sigma_i}{4\pi} [1 + \beta_i P_2(\cos \theta)] \quad (1)$$

where σ_i is the cross section, β_i is the asymmetry parameter, and θ is the angle between the electron's linear momentum and the direction of the light.

Calculating the photoionization parameters σ_i and β_i requires evaluation of the dipole matrix elements between the initial bound state Ψ_0^N and the final continuum state Ψ_{Ei}^N that describes the bound state Ψ_i^{N-1} and the photoelectron with energy E (all other quantum numbers are omitted for simplicity). At the single determinant level (IPA), employing a common set of orbitals $\{\phi_p\}$, describing both bound and continuum states,

$$\Psi_0^N = |\phi_1 \dots \phi_i \dots \phi_N\rangle \quad \text{and} \quad \Psi_{Ei}^N = |\phi_1 \dots \phi_E \dots \phi_N\rangle \quad (2)$$

we have

$$D_{E\alpha}^{0i} = \langle \Psi_{Ei}^N | D_\alpha | \Psi_0^N \rangle = \langle \phi_E | d_\alpha | \phi_i \rangle \quad (3)$$

where the subscript α indicates the electric dipole cartesian component. In the static DFT approach all orbitals are eigenstates of the ground state Kohn-Sham hamiltonian, h_{KS} ,⁵⁸

$$h_{\text{KS}}\phi_p = E_p\phi_p. \quad (4)$$

The one-particle Schrödinger equation can be solved accurately both for the bound and continuum states employing a B-spline basis and a Galerkin approach for the continuum eigenstates.^{59,60}

In general, occupied bound DFT orbitals are quite close to the Hartree-Fock ones. However, in critical cases, it is interesting to compare the results obtained using the DFT orbitals with those obtained employing the Hartree-Fock orbitals as initial orbitals in the Koopmans' description.

In fact, correlation effects in the bound states can be taken accurately into account by employing as initial orbital in Eq. (3) the Dyson orbital^{4,5,7} relative to the initial Ψ_0^N and final ionic state Ψ_i^{N-1} computed from highly correlated wavefunctions^{6,30,61,62}

$$\phi_i^d = \langle \Psi_i^{N-1} | \hat{\psi}(x) | \Psi_0^N \rangle = \sum_p \gamma_{ip} \phi_p; \quad \gamma_{ip} = \langle \Psi_i^{N-1} | a_p | \Psi_0^N \rangle \quad (5)$$

where $\hat{\psi}(x) = \sum_q \phi_q(x) a_q$ and a_p are field and orbital annihilator operators, respectively.⁴³ Thus,

$$D_{E\alpha}^{0i} = \langle \phi_E | d_\alpha | \phi_i^d \rangle. \quad (6)$$

Moreover, the squared norm of the Dyson orbital, defined as

$$R_i = \|\phi_i^d\|^2 = \sum_p \gamma_{ip}^2 \quad (7)$$

can be used as the intensities of the bands to simulate the photoelectron spectrum. R_i is known as pole strength, spectral strength, or spectroscopic factor of the final ionic state Ψ_i^{N-1} .

In this study, we use Dyson orbitals obtained at the equation of motion coupled cluster singles and doubles (EOM-CCSD) level of theory.^{6,41,42} Within EOM-CCSD theory, one has distinct left ($\phi_i^{d,L}$) and right ($\phi_i^{d,R}$) Dyson orbitals^{6,41,42}

$$\phi_i^{d,L} = \sum_p \gamma_{ip}^L \phi_p \quad \gamma_{ip}^L \equiv \langle \Psi_{0L}^N | a_p^\dagger | \Psi_{iR}^{N-1} \rangle \quad (8)$$

$$\phi_i^{d,R} = \sum_p \gamma_{ip}^R \phi_p \quad \gamma_{ip}^R \equiv \langle \Psi_{iL}^{N-1} | a_p | \Psi_{0R}^N \rangle \quad (9)$$

In the case of ionization from the electronic ground state

$$\gamma_{ip}^L = \langle \text{HF} | L^{\text{IP}} e^{(-T_2 - T_1)} a_p e^{(T_1 + T_2)} | \text{HF} \rangle \quad (10)$$

$$\gamma_{ip}^R = \langle \text{HF} | (1 + \hat{\Lambda}) e^{(-T_2 - T_1)} a_p^\dagger R^{\text{IP}} e^{(T_1 + T_2)} | \text{HF} \rangle \quad (11)$$

where we adopted standard EOM-CCSD notation,⁶³

$$\hat{\Lambda} = \sum_{\lambda_i = \lambda_1, \lambda_2} \bar{t}_{\lambda_i} \tau_{\lambda_i}^\dagger \quad (12)$$

$$R^{\text{IP}} = \sum_i r_i a_i + \frac{1}{2} \sum_{aij} r_{ij}^a a_a^\dagger a_j a_i. \quad (13)$$

Since right and left Dyson orbitals are different in EOM-CC, we here use as EOM-CC spectroscopic factors the dot product of the left and right Dyson orbital pairs,⁴³

$$R_i = \sum_p (\gamma_{ip}^L \gamma_{ip}^R). \quad (14)$$

The individual products $\gamma_{ip}^L \gamma_{ip}^R$ will be used as weights for specific p orbital contributions to a given ionisation i .

Because of the non-variational nature of CC, the calculation of the photoelectron transition dipole matrix element, Eq. (6), also requires generalization. As discussed in the SI of ref. 42, the transition strength (matrix element) between initial state 0 and final state i is written as (we omit the subscript E for ease of notation)

$$S_{\alpha\beta}^{0i} = \frac{1}{2} \{ D_\alpha^{0i} D_\beta^{i0} + (D_\beta^{0i} D_\alpha^{i0})^* \} \quad (15)$$

where the left and right moments are

$$D_\alpha^{0i} = \langle \Psi_0 | d_\alpha | \Psi_i \rangle^L; \quad D_\alpha^{i0} = \langle \Psi_i | d_\alpha | \Psi_0 \rangle^R. \quad (16)$$

The labels L or R highlight once again that in EOM-CC the above are not true scalar products, since they are not Hermitian, $D_{L,\alpha}^{i0} \neq (D_{R,\alpha}^{0i})^*$. We then write

$$D_{L,\alpha}^{i0} = \langle \phi_i^{d,L} | d_\alpha | \phi_E \rangle ; \quad D_{R,\alpha}^{i0} = \langle \phi_E | d_\alpha | \phi_i^{d,R} \rangle \quad (17)$$

The transition moments in Eq. (17) are now true scalar products (as computed in our program Tiresia⁶⁴) between the continuum and the left and right Dyson orbitals. Using the above expressions, we then consider the photoelectron transition strength matrix

$$\begin{aligned} S_{\alpha\beta}^{i0} &\equiv \langle \Psi_i | d_\alpha | \Psi_0 \rangle \langle \Psi_0 | d_\beta | \Psi_i \rangle \\ &= \frac{1}{2} \left[\langle \phi_E | d_\alpha | \phi_i^{d,R} \rangle \langle \phi_i^{d,L} | d_\beta | \phi_E \rangle \right. \\ &\quad \left. + \left(\langle \phi_E | d_\beta | \phi_i^{d,R} \rangle \langle \phi_i^{d,L} | d_\alpha | \phi_E \rangle \right)^* \right] \\ &= \frac{1}{2} \left[\langle \phi_E | d_\alpha | \phi_i^{d,R} \rangle \langle \phi_E | d_\beta | \phi_i^{d,L} \rangle^* \right. \\ &\quad \left. + \langle \phi_E | d_\alpha | \phi_i^{d,L} \rangle \langle \phi_E | d_\beta | \phi_i^{d,R} \rangle^* \right] \end{aligned} \quad (18)$$

Thus, in practice, any expression in our code for the cross section (originally written for variational wavefunctions⁶⁴) that contains Hermitian products of two dipole matrix elements is transformed, in the non-variational CC case, as

$$D_\alpha^{i0} (D_\beta^{i0})^* \rightarrow \frac{1}{2} \{ D_{R,\alpha}^{i0} D_{L,\beta}^{0i*} + D_{L,\alpha}^{i0} D_{R,\beta}^{0i*} \} \quad (19)$$

where α and β refer to different Cartesian components x , y or z . We refer to our previous studies^{42,43,61} for further details.

A step further is to include multielectron effects in the continuum states. A full treatment requires in principle the use of a close-coupling approach (equivalent to CI in the continuum), which is expensive and typically restricted to relatively small systems. A practical approximation is to include the response effects induced by the electromagnetic field on the electron cloud. This effect is well described by TDDFT (or RPA in ab initio) and in practice amounts to substituting the bare dipole operator d_α with the self-consistent potential (or dressed dipole) operator V_α^{SCF} in the evaluation of dipole matrix elements,^{43,44,65}

$$\langle \phi_E | V_\alpha^{\text{SCF}} | \phi_i \rangle . \quad (20)$$

Despite being computationally much more demanding, continuum TDDFT is still practical for rather large and complex molecules.⁴³

Summarizing, we have three choices for the initial orbital ϕ_i in Eq. (3), i.e., DFT and HF molecular orbital (MO) or EOM-CCSD Dyson, and two for the continuum states, either static DFT or TDDFT. The combination of the EOM-CCSD Dyson with the TDDFT continuum provides the most accurate description. For further computation details, see ESI, Section S2.

The epichlorohydrin molecule has conformational flexibility, with three stable conformers, denominated g-I,

g-II and cis,^{40,66} of which g-II is the dominant one. The three conformers are shown in Fig. S2, ESI.

All results reported are averages over those obtained for the separate conformers, with appropriate statistical weights (see Section S1 in ESI for more details).

III. RESULTS AND DISCUSSION

We remind the reader that epichlorohydrin is a closed shell molecule with 48 electrons, hence the highest occupied molecular orbital (HOMO) is number 24, HOMO-1 is number 23, and so on. In the following, we will label the final ionic states by the orbital from which we ionize according to the single determinant description, which is exact for the DFT or HF treatment. In the Dyson case, however, the same label will be associated to the actual wavefunction, starting from the lowest-energy ionic state. Thus, the ionisation energies will be labelled as 1A, 2A, 3A, \dots , and the corresponding Dyson orbitals (and channels) as 24a, 23a, 22a, \dots , with ‘‘A’’/‘‘a’’ indicating the symmetry irrep of the ionic state/ionised orbital.

A. Electronic Structure

Ionization energies and pole strengths computed at the EOM-IP-CCSD/aug-cc-pVDZ level for the three conformers are reported in Table I, together with experimental values for the IE’s from Ref. 40. We note that the pole strength values are large and close to 0.9 for all ionizations. These should not be confused with the height of the peaks in the experimental PE spectra, that depends on the photon energy at which the PE spectra are recorded.

TABLE I. $\text{C}_3\text{H}_5\text{OCl}$. Ionization energies (IE, eV) and intensities (pole strengths R_i) computed using EOM-IP-CCSD/aug-cc-pVDZ. Experimental values from Ref. 40. We also indicate, in parentheses, the ‘‘orbital label’’ assigned to the Dyson orbital corresponding to each ionisation.

| Ionis. i (Dyson) | cis | | g-I | | g-II | | Expt. IE ⁴⁰ |
|-----------------------|-------|--------|-------|--------|-------|--------|------------------------|
| | IE | R_i | IE | R_i | IE | R_i | |
| 1A (24a) | 10.29 | 0.8917 | 10.48 | 0.8917 | 10.51 | 0.8906 | 10.56 |
| 2A (23a) | 11.00 | 0.9082 | 11.03 | 0.9062 | 11.16 | 0.9096 | 11.28 |
| 3A (22a) | 11.32 | 0.9052 | 11.13 | 0.9056 | 11.41 | 0.9051 | 11.55 |
| 4A (21a) | 11.68 | 0.9005 | 11.72 | 0.9013 | 11.65 | 0.9005 | 11.81 |
| 5A (20a) | 13.49 | 0.9046 | 13.79 | 0.8983 | 13.61 | 0.8970 | 13.54 |
| 6A (19a) | 13.80 | 0.8922 | 14.03 | 0.8980 | 13.99 | 0.9045 | 14.16 |
| 7A (18a) | 14.62 | 0.8999 | 14.55 | 0.8977 | 15.13 | 0.8946 | 15.01 |
| 8A (17a) | 16.06 | 0.8935 | 15.79 | 0.8952 | 15.49 | 0.8941 | 15.64 |
| 9A (16a) | 16.43 | 0.8876 | 16.67 | 0.8861 | 16.59 | 0.8861 | 16.49 |
| 10A (15a) | 17.68 | 0.8791 | 17.68 | 0.8805 | 17.70 | 0.8821 | 17.47 |

As can be seen, the change from one conformer to the other is not negligible, up to a few tenths of an eV. The ionisation energies computed for the dominant g-II conformer compare pretty well with the experimental ones. HF and DFT eigenvalues are reported in Table S1 (ESI).

The Dyson orbital composition in terms of HF MOs is displayed in Table II. Table S2 reports the atomic 2p (and Cl 3p) populations of the HF MO (other populations, with the exception of H 1s, are very small and therefore omitted).

TABLE II. Epichlorohydrin. Highest coefficients γ_p^L, γ_p^R for each ionization channel. Numbers in parentheses labeled ‘HF’ denote the Hartree-Fock molecular orbitals contributing to the given ionization/Dyson orbital. Only contributions greater than 0.1 are reported.

| Ionis. (Dyson) | cis | g-I | g-II |
|-------------------|---|---|---------------------------------|
| 1A (24a) | 0.198(HF 21a) +0.108(HF 22a) +0.267(HF 23a) +0.307(HF 24a) | 0.304(HF 21a) +0.250(HF 22a) +0.244(HF 24a) | 0.376(HF 21a) +0.455(HF 23a) |
| 2A (23a) | 0.373(HF 23a) +0.513(HF 24a) | 0.312(HF 23a) +0.526(HF 24a) | 0.884(HF 24a) |
| 3A (22a) | 0.133(HF 21a) +0.461(HF 22a) +0.238(HF 23a) +0.132(HF 24a) | 0.110(HF 21a) +0.151(HF 22a) +0.510(HF 23a) | 0.425(HF 21a) +0.424(HF 23a) |
| 4A (21a) | 0.544(HF 21a) +0.313(HF 22a) | 0.438(HF 21a) +0.455(HF 22a) | 0.822(HF 22a) |
| 5A (20a) | 0.883(HF 20a) | 0.834(HF 20a) | 0.874(HF 20a) |
| 6A (19a) | 0.885(HF 19a) | 0.114(HF 18a) +0.718(HF 19a) | 0.887(HF 19a) |
| 7A (18a) | 0.871(HF 18a) | 0.773(HF 18a) +0.108(HF 19a) | 0.838(HF 18a) |
| 8A (17a) | 0.861(HF 17a) | 0.885(HF 17a) | 0.850(HF 17a) |
| 9A (16a) | 0.844(HF 16a) | 0.874(HF 16a) | 0.872(HF 16a) |

The Dyson orbitals of the first four ionised states show a heavy mixing of the four outermost (e.g., 24a, 23a, 22a and 21a) Hartree-Fock MO’s, while those of the inner ones have mostly pure, unmixed character, except minor mixing for 6A (19a) and 7A (18a) in g-I. Also, HF MO’s populations change significantly from one conformer to the other, although Cl 3p always dominates orbitals 24a and 23a, which are essentially Cl lone pairs. They seem to indicate a corresponding softness of the orbital composition, such that even modest conformational changes induce significant variations in individual orbitals. The final Dyson orbitals, on the other hand, appear more robust, as evidenced by the relatively modest changes in the β profiles evaluated for the three conformers in Fig. S3.

B. Photoelectron angular distribution measurements

The anisotropy parameters $\beta_i(h\nu)$ associated with epichlorohydrin’s outer valence PhotoElectron (PE) bands observed in the 10–19 eV IE range, have been studied experimentally and theoretically as a function of photon energy. Pairs of PE spectra recorded at two different angles, $\theta = 0^\circ$ and $\theta = 54.7^\circ$, from which the β values have been derived (see Section II and Section S1, ESI, for details), are reported in Fig. 1 for a representative set

of photon energies.

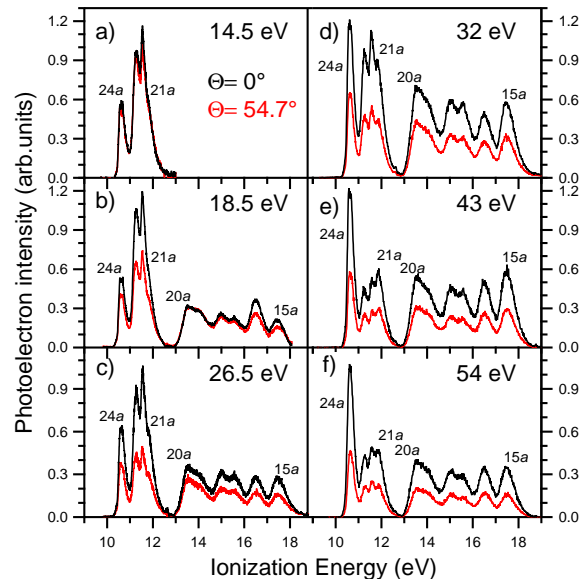


FIG. 1. Experimental outer valence PE spectra of epichlorohydrin recorded at the magic angle $\theta = 54.7^\circ$ (red) and $\theta = 0^\circ$ (black), and at different photon energies (panels a-f).

C. Anisotropy β

The experimental $\beta_i(h\nu)$ values of the outermost valence ionizations 24a–21a are reported in Fig. 2 and Fig. 3 (black dots in panels a-d), together with the simulated results. The latter differ in the continuum description, being DFT in Fig. 2 and TDDFT in Fig. 3.

The dynamical behaviors of the experimental β parameters, shown in Fig. 2, display clear similarities in the low energy region. All the β values are slightly negative or nearly zero at threshold, and rapidly increase with photon energy to reach, at 30 eV, largely positive values of approximately +1.0. A steeper increase is observed for the 23a and 22a channels with a change in slope at around 32 eV. Here, a maximum is located which corresponds to β values of +1.1 (23a) and +1.35 (22a). These two curves are the only ones exhibiting an oscillatory behaviour. This is characterized by a high-energy minimum which is measured for both channels at approximately 43 eV (see panels b and c in Fig. 2 and Fig. 3). Worth noting is the difference between the two channels in the β oscillation amplitude, namely the maximum-to-minimum β change, these amplitudes being 0.3 and 0.5 for 23a and 22a, respectively. A change in slope in the β curve at 32eV is also observed for the other two photoionization processes 24a and 21a. While the slope change is modest for the 24a channel, the change observed is instead large in the 21a curve, where a clear plateau appears in the 30–43 eV photon energy region with $\beta = +1.0$. The β increase at low energies for the first four PE bands is

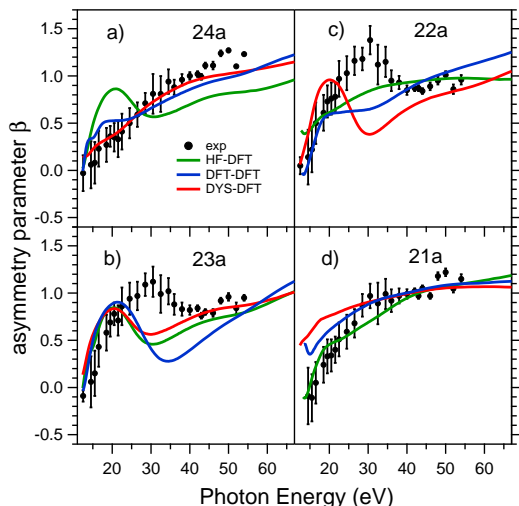


FIG. 2. Asymmetry parameters β_i as a function of the photon energy for orbitals (channels) 24a, 23a, 22a and 21a. Experiment versus computational results obtained using a DFT representation of the continuum together with Hartree-Fock (label HF-DFT), Density Function Theory (label DFT-DFT) and EOM-CCSD Dyson (label DYS-DFT) orbitals.

also evident in Fig. 1. Here, isotropic β values, $\beta=0$, are measured at 14.5 eV (panel a), as the spectra recorded at 0° and 54.7° almost perfectly coincide. In going from 14.5 to 32eV, from panel a to panel d, the relative intensities of these bands in the 0° spectra clearly display a gradual increase, which corresponds to the β monotonic increase quoted in the panels of Fig. 2 at low energies. The $\beta_i(h\nu)$ parameters have also been measured for the other outer valence ionizations 20a–15a (see ESI). They do not exhibit an oscillatory behaviour and show an increase similar to those of 24a and 21a channels, reaching values in the range 0.9-1.2 at 54 eV photon energy.

In Fig. 2 are also shown the computational results relative to the same DFT continuum, but with different initial orbitals, DFT, HF and EOM-CCSD Dyson (labelled DYS). The marked differences show the sensitivity of the calculated asymmetry parameter to the bound-state description, and in particular between HF and DFT orbitals, which are generally believed to be quite close to each other. The most notable difference is the position of the maximum and of the oscillation expected from the CM effect. With HF orbitals, the CM feature appears strong in the HOMO (24a) and in the 23a channel, with comparable amplitude. DFT shows instead a small hint of it in 24a, another inflection in 22a, and a very strong oscillation in 23a. The use of Dyson orbitals correctly displays the CM feature in the 22a and 23a channels, and follows the experimental trend with a larger amplitude in 22a compared with 23a. In all cases the energy positions of the maximum and the minimum are strongly shifted towards threshold, by almost 10 eV. For 21a all approaches are qualitatively correct, with no sign of CM feature. Here, HF gives the best agreement at low energy,

while both DFT and Dyson results are overestimated; then at higher energy the shape favours the latter. A good agreement with experiment is obtained from the Dyson results for the HOMO (24a), and for the steep rise at low energy in channels 22a and 23a. Due to the energy shift of the CM feature, it is difficult to argue for the intermediate energy region.

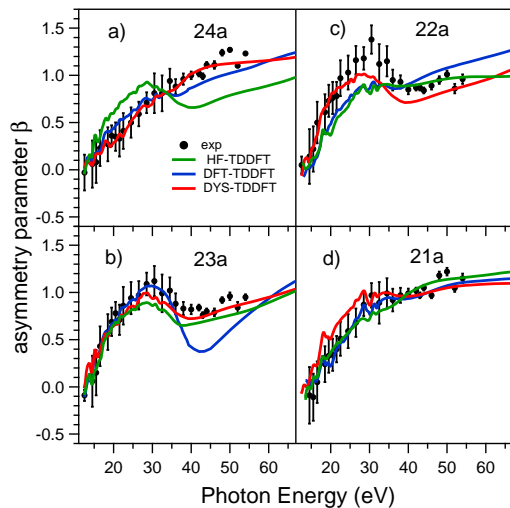


FIG. 3. Asymmetry parameters β_i as a function of the photon energy for orbitals (channels) 24a, 23a, 22a and 21a. Experiment versus computational results obtained using a TDDFT representation of the continuum together with Hartree-Fock (HF-TDDFT), Density Function Theory (DFT-TDDFT) and EOM-CCSD Dyson (DYS-TDDFT) orbitals.

TDDFT continuum strongly improves the position of the CM feature, as is displayed in Fig. 3 for the same three descriptions of the bound states. The improvements brought about by the TDDFT continuum are, in fact, dramatic. This has been observed long ago in the case of rare gas atoms,^{65,67} and in small molecules containing second row elements, like PH_3 or Cl_2 .^{44,68} In the present case, the agreement of the EOM-CCSD Dyson/TDDFT approach is almost quantitative. The energy positions of the CM maximum and minimum are now correct, as correct is the range of the oscillation, perhaps only slightly underestimated for the 22a ionization. Also the overall shapes, including the shape of the low energy rising leg and the high energy behaviour, are very well reproduced. Even the behaviour of the other curves (DFT and HF) is improved, due to the correct energy position of the CM feature, although the shortcomings already noted, i.e., the misplacing of the CM feature in 24a by the HF orbitals, the overestimate of it in 23a by DFT, and the underestimate by both HF and DFT in 22a, are of course unchanged. The high energy slope is also not well reproduced in some cases.

To summarize, the use of the TDDFT continuum is paramount to obtain the correct location of the CM feature, and it generally improves the overall description of the β profiles. The location and amplitude of the oscilla-

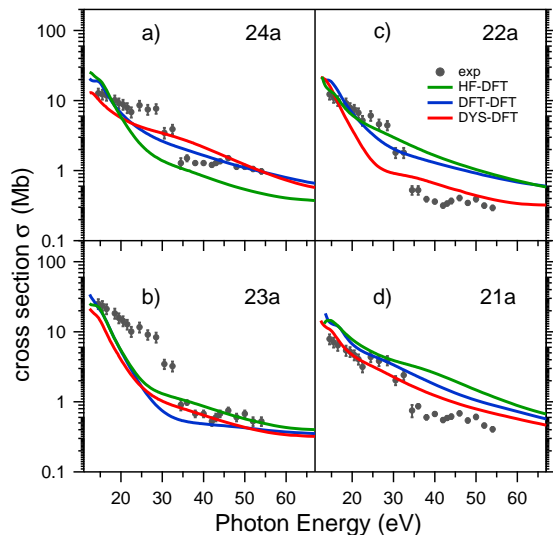


FIG. 4. Cross section σ (Mb, logarithmic scale) as a function of the photon energy for orbitals 24, 23, 22 and 21. Experiment versus computational results obtained using a DFT representation of the continuum together with Hartree-Fock (HF-DFT), Density Function Theory (DFT-DFT) and EOM-CCSD Dyson (DYS-DFT) orbitals.

tion are entirely due to the nature of the initial orbitals, and specifically their AO composition, and give a very clear experimental signature of the orbital rotation effect upon ionization theoretically predicted.⁸

D. Partial cross sections

The behaviour of the cross sections tells a similar story, although less vivid. As before, experimental results and theoretical curves relative to the DFT continuum are reported in Fig. 4.

Again, two different behaviours are observed experimentally for channels 22a and 23a, where a sudden drop in σ is seen in the region of the CM, around 40 eV, and for 21a, 24a, where the decrease is smoother. Note also the slight (log scale) but well visible recovery of the cross section after the CM. As before, HF results show the step-like decline in the HOMO 24a while it misses it in 22a. DFT also misses it in 22a while it exaggerates it in 23a, basically shifting most Cl 3p contribution to this ionization. The cross-section decrease in 21a is smoother in all approaches, and the same occurs for DFT and Dyson also for 24a. One could expect that the CM feature were propagated from 23a, 22a, where it is native due to the Cl 3p participation, to the neighboring channels due to interchannel coupling, absent in DFT but included in the TDDFT continuum. However, this is not borne out, as seen in Fig. 5, where TDDFT vastly improves the description of 22a and 23a while the effect is less marked for 24a and 21a, as TDDFT mostly affects the CM feature.

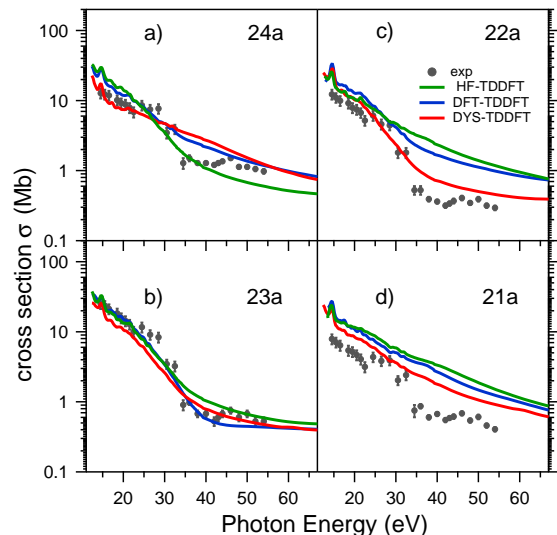


FIG. 5. Cross section σ (Mb) as a function of the photon energy for orbitals 24a, 23a, 22a and 21a. Experiment versus computational results obtained using a TDDFT representation of the continuum together with Hartree-Fock (HF-TDDFT), Density Function Theory (DFT-TDDFT) and EOM-CCSD Dyson (DYS-TDDFT) orbitals.

There is no sign of the cross section intensity recovery after the minimum. Since this feature is more or less similar in all experimental channels, it may not be significant, and no clear signs of interchannel coupling effects appear also in the experiment. Clearly, the overall final agreement is less good than for the β values. Moreover, experiment seems to indicate more structure than is theoretically predicted. It should be mentioned that the experimental measurement of cross sections is intrinsically more difficult than that of the β parameters, and that the CM effect in cross sections manifests itself as a much weaker relative intensity change. As a consequence, it is more difficult to be described theoretically. Since only relative cross sections have been experimentally measured, a conversion to absolute scale was required to make a direct comparison between experiment and theory possible (see Fig. 4 and Fig. 5). The conversion factor was determined by comparing the sum of the experimental cross sections of the 24a ionization channel measured at all the selected photon energies to the sum of the corresponding theoretical values calculated by the Dyson-TDDFT method.

An alternative presentation of the comparison between experimental and theoretical cross sections, which eliminates the ambiguity in the absolute values, is the use of branching ratios (BR), i.e. in the present case the ratio of individual channel cross section to their sum relative to the four channels considered. Experimental and theoretical values relative to the TDDFT continuum are reported in Fig. 6, and those corresponding to the DFT continuum are available in the ESI (see Fig. S7).

The drawback of the BR is that a strong resonant fea-

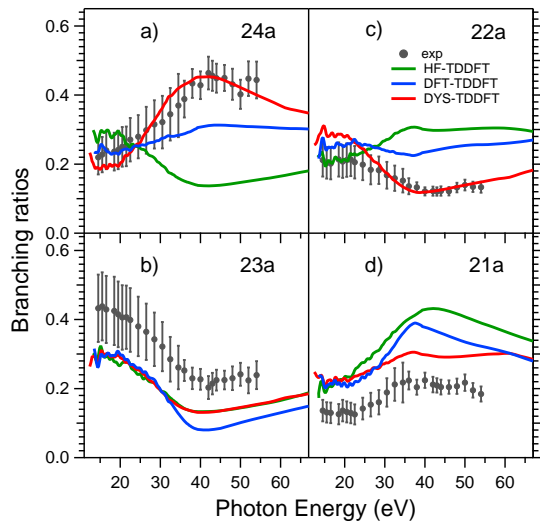


FIG. 6. Branching ratios for orbitals 24a, 23a, 22a and 21a as a function of the photon energy. Experiment versus computational results obtained using a TDDFT representation of the continuum together with Hartree-Fock (HF-TDDFT), Density Function Theory (DFT-TDDFT) and EOM-CCSD Dyson (DYS-TDDFT) orbitals.

ture present in one channel influences all the others, so that even a channel with a smooth cross section will display induced features. The upside is that spurious fluctuations in the cross sections cancel out, and the profiles are cleaner and independent on normalization. In Fig. 6 the difference between the alternative descriptions is very clear, and the same features already discussed for each channel appear prominently. An excellent description is provided by the DYS-TDDFT approach for the 24a and 22a channels. For the 23a and 21a ones, the shape is very well reproduced, but the ratio is underestimated for 23a and correspondingly overestimated for 21a. While an obvious suggestion is a difficulty in the deconvolution of partially overlapping bands, of different widths and shape, we do not have presently an unequivocal attribution of this disagreement either to a deficiency of the processing of experimental data or the inadequacy of the theoretical approach.

A brief analysis of the remaining ionizations, 15a-20a is presented in ESI, see Section S3.

IV. CONCLUSIONS

Photoionization cross sections σ and angular distributions β have been accurately measured for the entire outer valence region of the chiral molecule epichlorohydrin over an extended energy range, which is important to fully characterize specific signatures. Prominent features in the β parameters appear in two of the four outermost ionizations, attributed to Cooper Minimum effects linked to a Cl 3p participation in the relevant orbitals.

Detailed theoretical calculations employing DFT, HF and Dyson orbitals computed at the EOM-CCSD level provide different energy positions of the Cooper Minimum features in the β parameters, a clear signature of important correlation effects upon ionization, only observable in transition properties like photoionization dynamical parameters. Such effects, predicted long ago but never observed, do not show up in ionisation energies or pole strengths, which remain close to 1, so they are not due to a *breakdown of the one-particle picture* (as defined by Cederbaum), but represent an *orbital mixing*, or *orbital rotation upon ionization* caused by differential relaxation and correlation upon ionization. The use of the TDDFT continuum is essential for the proper energy prediction (i.e. its position on the energy axis) of the Cooper Minimum and, in general, coupling the TDDFT continuum to the Dyson orbital description of the bound initial and final states provides a very accurate description of the experimental results. Although less prominent, such orbital mixing effects also manifest themselves in the cross section and in the branching ratios. While their shapes are very well described by theoretical results, a discrepancy in some absolute values is apparent, whose origin is not clear at present. Additional discrepancies between DFT and HF initial orbitals are also of interest, and clearly highlighted by the present results, which are shown to be highly informative on the electronic structure of the molecule. Although less dramatic, such effects are also seen in the remaining part of the valence shell.

To conclude we note that, because of the lack of symmetry and the dense manifold of valence orbitals in chiral molecules, such orbital mixing effects are expected to be relatively common in their photoionization properties, and in particular in their PECD spectra, as already observed in Ref. 15, for which the present methodology is expected to provide an accurate description. Although the dichroic parameter β_1 decreases fast with increasing electron kinetic energy and is therefore a less sensitive probe of the CM, it will probably be strongly affected by the orbital rotation.¹⁵ Since theoretical simulations of PECD, like in conventional CD, are almost mandatory to interpret the observed signal, the present study has strong implication for future PECD studies. Further investigations in this regard are in progress.

ACKNOWLEDGMENTS

The authors gratefully acknowledge the staff of ELETTRA for the smooth operation of the storage ring during the measurements. S.S. thanks Sapienza University for financial support through Progetto Ateneo Medio 2023, RM123188F6672F66 L.S. acknowledges financial support by IOM-CNR (research grant), SBAI Department of Sapienza (PhD grant) and Sapienza University for a research grant (prot.n. AR11715C81FF05FF). S.C. thanks the Hamburg Cluster of Excellence ‘‘CUI: Advanced Imaging of Matter’’ for the 2024 Mildred Dres-

selhaus Prize. T.M. and S.C. acknowledge the Marie Skłodowska-Curie European Training Network COmputational Spectroscopy In Natural sciences and Engineering (COSINE), Grant Agreement No. 765739.

SUPPORTING INFORMATION

S1 Spectral extraction of the experimental β parameters; S2 Computational Details; S3 Higher energy ionizations (deeper ionisations); S4 Cartesian coordinates of the three rotamers (Bohr units); S5 Additional Tables and Figures; S6 Comparison between experimental and theoretical observables; S7 Derivation of β_{av} over conformers.

DATA AVAILABILITY

In addition to the details given in the manuscript and ESI file, all data underlying this study are available from the authors upon reasonable request.

REFERENCES

- F. I. Vilesov, B. L. Kurbatov, and A. N. Terenin, "Energy distribution of electrons in photoionization of aromatic amines in the gaseous phase," *Soviet physics. Doklady* **6**, 490 (1961).
- K. Siegbahn, C. Nordling, G. Johansson, J. Hedman, P. F. Heden, K. Hamrin, U. Gelius, T. Bergmark, L. O. Werme, R. Manne, and Y. Baer, *ESCA applied to free molecules* (North-Holland, Amsterdam, 1969).
- D. W. Turner and M. I. A. Jobory, "Determination of Ionization Potentials by Photoelectron Energy Measurement," *J. Chem. Phys.* **37**, 3007–3008 (1962).
- B. T. Pickup, "On the theory of fast photoionization processes," *Chem. Phys.* **19**, 193–208 (1977).
- R. Arneberg, J. Müller, and R. Manne, "Configuration interaction calculations of satellite structure in photoelectron spectra of H₂O," *Chem. Phys.* **64**, 249–258 (1982).
- C. M. Oana and A. I. Krylov, "Dyson orbitals for ionization from the ground and electronically excited states within equation-of-motion coupled-cluster formalism: Theory, implementation, and examples," *J. Chem. Phys.* **127**, 234106 (2007).
- J. V. Ortiz, "Dyson-orbital concepts for description of electrons in molecules," *J. Chem. Phys.* **153**, 070902 (2020).
- W. Von Niessen, G. Bieri, J. Schirmer, and L. Cederbaum, "Hole-mixing effects in the ionization of some unsaturated oxo-compounds," *Chem. Phys.* **65**, 157–176 (1982).
- A. I. Kuleff and L. S. Cederbaum, "Ultrafast correlation-driven electron dynamics," *J. Phys. B: Atom. Molec. Opt. Phys.* **47**, 124002 (2014).
- L. S. Cederbaum, J. Schirmer, W. Domcke, and W. Von Niessen, "On the adequacy of the molecular-orbital picture for describing ionization processes," *Int. J. Quantum Chem.* **14**, 593–601 (1978).
- L. S. Cederbaum, W. Domcke, J. Schirmer, and W. Von Niessen, "Correlation effects in the ionization of molecules: Breakdown of the molecular orbital picture," *Adv. Chem. Phys.* **65**, 115–159 (1986).
- M.-M. Rohmer and A. Veillard, "Photoelectron spectrum of bis-(π -allyl)nickel," *J. Chem. Soc., Chem. Commun.* , 250–251 (1973).
- V. Despré, N. V. Golubev, and A. I. Kuleff, "Charge migration in propiolic acid: A full quantum dynamical study," *Phys. Rev. Lett.* **121**, 203002 (2018).
- B. Mignolet, R. D. Levine, and F. Remacle, "Charge migration in the bifunctional penna cation induced and probed by ultrafast ionization: a dynamical study," *J. Phys. B: At. Mol. Opt. Phys.* **47**, 124011 (2014).
- M. D. J. Waters, N. Ladda, A. Senftleben, V. Svoboda, M. Belozertsev, T. Baumert, and H. J. Wörner, "Ground-state photoelectron circular dichroism of methyl p-tolyl sulfoxide by single-photon ionisation from a table-top source," *ChemPhysChem* **23**, e202200575 (2022).
- J. W. Cooper, "Photoionization from outer atomic subshells. a model study," *Phys. Rev.* **128**, 681–693 (1962).
- S. T. Manson and J. W. Cooper, "Photo-ionization in the soft x-ray range: 1z dependence in a central-potential model," *Phys. Rev.* **165**, 126–138 (1968).
- R. G. Houlgate, K. Codling, G. V. Marr, and J. B. West, "Angular distribution and photoionization cross section measurements on the 3p and 3s subshells of argon," *J. Phys. B: Atom. Mol. Phys.* **7**, L470–L473 (1974).
- R. G. Houlgate, J. B. West, K. Codling, and G. V. Marr, "The angular distribution of the 3p electrons and the partial cross section of the 3s electrons of argon from threshold to 70 eV," *J. Electron Spectrosc. Relat. Phenom* **9**, 205–209 (1976).
- D. L. Miller, J. D. Dow, R. G. Houlgate, G. V. Marr, and J. B. West, "The photoionisation of krypton atoms: a comparison of pseudopotential calculations with experimental data for the 4p asymmetry parameter and cross section as a function of the energy of the ejected photoelectrons," *J. Phys. B: Atom. Mol. Phys.* **10**, 3205 (1977).
- L. Torop, J. Morton, and J. B. West, "The angular distribution of photoelectrons from xenon," *J. Phys. B: Atom. Mol. Phys.* **9**, 2035 (1976).
- T. A. Carlson, M. O. Krause, F. A. Grimm, P. Keller, and J. W. Taylor, "Angle-resolved photoelectron spectroscopy of CCl₄: The Cooper minimum in molecules," *J. Chem. Phys.* **77**, 5340–5347 (1982).
- T. A. Carlson, M. O. Krause, and F. A. Grimm, "Angle resolved photoelectron spectroscopy of CS₂ and COS measured as a function of photon energy from 21 to 70 eV," *J. Chem. Phys.* **77**, 1701–1709 (1982).
- T. A. Carlson, M. O. Krause, F. A. Grimm, and T. A. Whitley, "Angle-resolved photoelectron spectroscopy of Cl₂ as a function of photon energy from 18 to 70 eV," *J. Chem. Phys.* **78**, 638–642 (1983).
- T. A. Carlson, M. O. Krause, A. Fahlman, P. R. Keller, J. W. Taylor, T. Whitley, and F. A. Grimm, "Angle-resolved photoelectron spectroscopy of HCl from a photon energy of 16 to 80 eV," *J. Chem. Phys.* **79**, 2157–2162 (1983).
- T. A. Carlson, A. Fahlman, M. O. Krause, T. A. Whitley, F. A. Grimm, M. N. Piancastelli, and J. W. Taylor, "Angle-resolved photoelectron spectroscopy of the valence orbitals of SiCl₄ as a function of photon energy from 14 to 80 eV," *J. Chem. Phys.* **84**, 641–648 (1986).
- T. A. Carlson, M. O. Krause, W. A. Svensson, P. Gerard, F. A. Grimm, T. A. Whitley, and B. P. Pullen, "Photoelectron Dynamics of the Cooper Minimum in Free Molecules," *Z. Phys. D, Atom. Mol. Clusters* **2**, 309–318 (1986).
- A. W. Potts, I. Novak, F. Quinn, G. V. Marr, B. Dobson, I. H. Hillier, and J. B. West, "Photoelectron asymmetry measurements for CFCl₃, CF₂Cl₂ and CF₃Cl in the photon energy range 18–80 eV," *J. Phys. B: At. Mol. Opt. Phys.* **18**, 3177 (1985).
- W. Thiel, "Theoretical analysis of photoelectron angular distributions in hydrogen chloride," *J. Electron Spectrosc. Relat. Phenom.* **34**, 399–405 (1984).
- A. Ponzi, C. Angeli, R. Cimraglia, S. Coriani, and P. Decleva, "Dynamical photoionization observables of the cs molecule: the role of electron correlation." *J. Chem. Phys.* **140** **20**, 204304 (2014).

- ³¹D. M. P. Holland, D. Edvardsson, L. Karlsson, R. Maripuu, K. Siegbahn, A. W. Potts, and W. von Niessen, "An experimental and theoretical study of the valence shell photoelectron spectrum of bromobenzene," *Chem. Phys.* **252**, 257–278 (2000).
- ³²I. Powis, D. M. P. Holland, E. Antonsson, M. Patanen, C. Nicolas, C. Miron, M. Schneider, D. Y. Soshnikov, A. Dreuw, and A. B. Trofimov, "The influence of the bromine atom cooper minimum on the photoelectron angular distributions and branching ratios of the four outermost bands of bromobenzene," *J. Chem. Phys.* **143**, 144304 (2015).
- ³³I. Powis, M. Patanen, E. Antonsson, C. Nicolas, C. Miron, and D. M. P. Holland, "Vibration-dependent photoelectron angular distributions and branching ratios observed across the cooper-minimum region of bromobenzene," *Phys. Rev. A* **96**, 013413 (2017).
- ³⁴G. A. Garcia, H. Dossmann, L. Nahon, S. Daly, and I. Powis, "Photoelectron circular dichroism and spectroscopy of trifluoromethyl- and methyl-oxirane: a comparative study," *Phys. Chem. Chem. Phys.* **16**, 16214–16224 (2014).
- ³⁵S. Stranges, S. Turchini, M. Alagia, G. Alberti, G. Contini, P. Decleva, G. Fronzoni, M. Stener, N. Zema, and T. Prospero, "Valence photoionization dynamics in circular dichroism of chiral free molecules: The methyl-oxirane," *J. Chem. Phys.* **122**, 244303 (2005).
- ³⁶S. Turchini, N. Zema, G. Contini, G. Alberti, M. Alagia, S. Stranges, G. Fronzoni, M. Stener, P. Decleva, and T. Prospero, "Circular dichroism in photoelectron spectroscopy of free chiral molecules: Experiment and theory on methyl-oxirane," *Phys. Rev. A* **70**, 014502 (2004).
- ³⁷G. Alberti, S. Turchini, G. Contini, N. Zema, T. Prospero, S. Stranges, V. Feyer, P. Bolognesi, and L. Avaldi, "Dichroism in core-excited and core-ionized methyloxirane," *Physica Scripta* **78**, 058120 (2008).
- ³⁸B. A. McGuire, P. B. Carroll, R. A. Loomis, I. A. Finneran, P. R. Jewell, A. J. Remijan, and G. A. Blake, "Discovery of the interstellar chiral molecule propylene oxide ($\text{CH}_3\text{CHCH}_2\text{O}$)," *Science* **352**, 1449–1452 (2016).
- ³⁹S. Daly, I. Powis, G. A. Garcia, H. Soldi-Lose, and L. Nahon, "Photoionization of epichlorohydrin enantiomers and clusters studied with circularly polarized vacuum ultraviolet radiation," *J. Chem. Phys.* **134**, 064306 (2011).
- ⁴⁰S. Stranges, M. Alagia, P. Decleva, M. Stener, G. Fronzoni, D. Toffoli, M. Speranza, D. Catone, S. Turchini, T. Prospero, N. Zema, G. Contini, and Y. Keheyani, "The valence electronic structure and conformational flexibility of epichlorohydrin," *Phys. Chem. Chem. Phys.* **13**, 12517–12528 (2011).
- ⁴¹C. M. Oana and A. I. Krylov, "Cross sections and photoelectron angular distributions in photodetachment from negative ions using equation-of-motion coupled-cluster dyson orbitals," *J. Chem. Phys.* **131**, 124114 (2009).
- ⁴²T. Moitra, A. Ponzi, H. Koch, S. Coriani, and P. Decleva, "Accurate description of photoionization dynamical parameters," *J. Phys. Chem. Lett.* **11**, 5330–5337 (2020).
- ⁴³T. Moitra, S. Coriani, and P. Decleva, "Capturing correlation effects on photoionization dynamics," *J. Chem. Theory Comput.* **17**, 5064–5079 (2021).
- ⁴⁴M. Stener, G. Fronzoni, and P. Decleva, "Time-dependent density-functional theory for molecular photoionization with noniterative algorithm and multicenter B-spline basis set: CS_2 and C_6H_6 case studies," *J. Chem. Phys.* **122**, 234301 (2005).
- ⁴⁵P. Decleva, M. Stener, and D. Toffoli, "Continuum Electronic States: The Tiresia Code," *Molecules* **27**, 2026 (2022).
- ⁴⁶A. Derossi, F. Lama, M. Piacentini, T. Prospero, and N. Zema, "High flux and high resolution beamline for elliptically polarized radiation in the vacuum ultraviolet and soft x-ray regions," *Rev. Sci. Instr.* **66**, 1718–1720 (1995).
- ⁴⁷J. M. Dyke, D. Haggerston, A. Morris, S. Stranges, J. B. West, T. G. Wright, and A. E. Wright, "A study of the so molecule with photoelectron spectroscopy using synchrotron radiation," *J. Chem. Phys.* **106**, 821–830 (1997).
- ⁴⁸F. Innocenti, M. Eypper, S. Beccaceci, A. Morris, S. Stranges, J. B. West, G. C. King, and J. M. Dyke, "A Study of the Reactive Intermediate IF and I Atoms with Photoelectron Spectroscopy," *J. Phys. Chem. A* **112**, 6939–6949 (2008).
- ⁴⁹F. Innocenti, M. Eypper, E. P. F. Lee, S. Stranges, D. K. W. Mok, F.-t. Chau, G. C. King, and J. M. Dyke, "Difluorocarbene Studied with Threshold Photoelectron Spectroscopy (TPES): Measurement of the First Adiabatic Ionization Energy (AIE) of CF_2 ," *Chem. Eu. J.* **14**, 11452–11460 (2008).
- ⁵⁰L. Schio, M. Alagia, D. Toffoli, P. Decleva, R. Richter, O. Schalk, R. D. Thomas, M. Mucke, F. Salvador, P. Bertoch, D. Benedetti, C. Dri, G. Cautero, R. Sergio, L. Stebel, D. Vivoda, and S. Stranges, "Photoionization Dynamics of the Tetraoxo Complexes OsO_4 and RuO_4 ," *Inorg. Chem.* **59**, 7274–7282 (2020).
- ⁵¹J. Cooper and R. N. Zare, "Angular distribution of photoelectrons," *J. Chem. Phys.* **48**, 942–943 (1968).
- ⁵²S. Southworth, W. D. Brewer, C. M. Truesdale, P. H. Kobrin, D. W. Lindle, and D. A. Shirley, "Photoelectron angular distributions from H_2 and D_2 ," *J. Electron Spectrosc. Relat. Phenom.* **26**, 43–51 (1982).
- ⁵³T. Yu and H. Peng, "Quantification and deconvolution of asymmetric LC-MS peaks using the bi-Gaussian mixture model and statistical model selection," *BMC Bioinformatics* **11**, 559 (2010).
- ⁵⁴T. S. Buys and K. De Clerck, "Bi-gaussian fitting of skewed peaks," *Anal. Chem.* **44**, 1273–1275 (1972).
- ⁵⁵D. M. P. Holland, A. C. Parr, D. L. Ederer, J. L. Dehmer, and J. B. West, "The angular distribution parameters of argon, krypton and xenon for use in calibration of electron spectrometers," *Nucl. Instrum* **195**, 331–337 (1982).
- ⁵⁶J. Kreile and A. Schweig, "Photoelectron asymmetry parameters of Ar, Kr, Xe, H_2 , N_2 , O_2 , CO and CO_2 : New measurements and a reconsideration of literature data," *J. Electron Spectrosc. Relat. Phenom* **20**, 191–211 (1980).
- ⁵⁷J. L. Dehmer, W. A. Chupka, J. Berkowitz, and W. T. Jivry, "Wavelength dependence of the photoelectron angular distributions of the rare gases," *Phys. Rev. A* **12**, 1966–1973 (1975).
- ⁵⁸D. Toffoli, M. Stener, G. Fronzoni, and P. Decleva, "Convergence of the multicenter B-spline DFT approach for the continuum," *Chem. Phys.* **276**, 25–43 (2002).
- ⁵⁹M. Brosolo, P. Decleva, and A. Lisini, "LCAO expansion in a spline basis for accurate variational determination of continuum wavefunctions. Applications to H_2^+ and HeH^{2+} ," *Chem. Phys.* **181**, 85–95 (1994).
- ⁶⁰C. F. Fischer and M. Idrees, "Spline methods for resonances in photoionisation cross sections," *J. Phys. B: At. Mol. Opt. Phys.* **23**, 679–691 (1990).
- ⁶¹T. Moitra, A. C. Paul, P. Decleva, H. Koch, and S. Coriani, "Multi-electron excitation contributions towards primary and satellite states in the photoelectron spectrum," *Phys. Chem. Chem. Phys.* **24**, 8329–8343 (2022).
- ⁶²B. N. C. Tenorio, A. Ponzi, S. Coriani, and P. Decleva, "Photoionization Observables from Multi-Reference Dyson Orbitals Coupled to B-Spline DFT and TD-DFT Continuum," *Molecules* **27**, 1203 (2022).
- ⁶³J. F. Stanton and R. J. Bartlett, "The equation of motion coupled-cluster method. a systematic biorthogonal approach to molecular excitation energies, transition probabilities, and excited state properties," *J. Chem. Phys.* **98**, 7029–7039 (1993).
- ⁶⁴D. Toffoli, S. Coriani, M. Stener, and P. Decleva, "Tiresia: A code for molecular electronic continuum states and photoionization," *Comp. Phys. Comm.* **297**, 109038 (2024).
- ⁶⁵A. Zangwill and P. Soven, "Density-functional approach to local-field effects in finite systems: Photoabsorption in the rare gases," *Phys. Rev. A* **21**, 1561–1572 (1980).
- ⁶⁶M. C. Tam and T. D. Crawford, "Ab Initio Determination of Optical Rotatory Dispersion in the Conformationally Flexible Molecule (R)-Epichlorohydrin," *J. Phys. Chem. A* **110**, 2290–2298 (2006).
- ⁶⁷M. Stener, P. Decleva, and A. Lisini, "Density functional-time-dependent local density approximation calculations of autoion-

ization resonances in noble gases," *J. Phys. B: At. Molec. Opt. Phys.* **28**, 4973 (1995).

⁶⁸M. Stener and P. Decleva, "Time-dependent density functional calculations of molecular photoionization cross sections: N₂ and PH₃," *J. Chem. Phys.* **112**, 10871–10879 (2000).

Supplementary Information:
Evidence of orbital mixing upon ionization via Cooper minimum
photoelectron dynamics in epichlorohydrin. Experiment and Theory

L. Schio,^{a,b} M. Alagia,^a T. Moitra,^{c,d} D. Toffoli,^e A. Ponzi,^f M. Stener,^e
S. Coriani,^c P. Decleva,^{e,*} O. Rebrov,^g V. Zhaunerchyk,^h
M. Larsson,^g S. Falcinelli,ⁱ A. A. Dias,^j D. Catone,^k S. Turchini,^k
N. Zema,^l F. Salvador,^a D. Benedetti,^a D. Vivoda,^l B. Botta,^m and S. Stranges^{m,a,*}

^a CNR - Istituto Officina dei Materiali (IOM), Laboratorio TASC,
Area Science Park Basovizza, Trieste, Italy.

^b Department of Basic and Applied Science for Engineering (SBAI),
Sapienza University, Rome, Italy.

^c DTU Chemistry, Technical University of Denmark,
Kemitorvet 207, 2800 Kongens Lyngby, Denmark.

^d Department of Physical and Theoretical Chemistry, Faculty of Natural Sciences,
Comenius University, SK-84215, Bratislava, Slovakia

^e Dipartimento di Scienze Chimiche e Farmaceutiche,
Università degli Studi di Trieste, Trieste, Italy

^f Institut Ruder Bošković, Bijeniška cesta 54, 10000 Zagreb, Croatia

^g Department of Physics, University of Stockholm, Stockholm, Sweden

^h Department of Physics, University of Gothenburg, Gothenburg, Sweden

ⁱ Dipartimento di Ingegneria Civile ed Ambientale,
Università degli Studi di Perugia, Perugia, Italy

^j Laboratory for Instrumentation, Biomedical Engineering, and Radiation Physics,
Departamento de Física, Faculdade de Ciências e Tecnologia,
Universidade NOVA de Lisboa, Capacarica, Portugal

^k CNR-ISM, Area della Ricerca di Roma Tor Vergata,
Via del Fosso del Cavaliere 100, Roma, Italy

^l Elettra-Sincrotrone Trieste, Area Science Park, Basovizza, Trieste, Italy

^m Department of Chemistry and Technologies of Drugs,
Sapienza University, I-00183, Rome, Italy.

*Corresponding authors: decleva@units.it (theory), stefano.stranges@uniroma1.it (experiment)

S1 Spectral extraction of the experimental σ and β parameters

To extract the $\sigma(h\nu)$ and $\beta_i(h\nu)$ values from the spectrum, the relative intensities of the single PE components in terms of peak areas were obtained by the global multipeak fitting procedure¹ described below. First, the PE spectra were normalized by the photon flux and corrected by the proper spectrometer transmission function. The background contribution was then systematically removed from all the spectra using the following procedure. The background, as described by an `arctan` function plus a linear function, was determined by a χ -square based fitting of spectra recorded without epichlorohydrin, and subtracted from the total spectrum. The initial part of the step onset of this function was involved in the procedure. This subtraction, although applied to all spectra, was actually needed for a subset of PE spectra recorded at low photon energies, and proved especially significant in the low kinetic energy part of the spectrum. The net spectra, thus obtained, were analysed by a global multipeak fitting method,¹ which simultaneously involved the data obtained at all investigated photon energies, as well as at the 0° and 54.7° detection angles. Ten spectral components were considered, namely the PE bands associated with the ionizations from the 24a–15a MOs. The PE spectrum could be conveniently divided in two not overlapping regions. The first group of four bands, the 24a–20a components in the 10.0–13.0 eV IE range, could be analysed separately from the other bands. These four bands exhibit a variety of shapes and intensities, as well as different extent of overlap, as the photon energy is increased. In order to describe their envelopes and ionization potentials precisely and consistently, a program was developed which efficiently makes curve fits of the spectral data. Because all bands have an asymmetric shape, with longer tail on the high IE side (right side), an asymmetric Gaussian was adopted, namely a set of bi-Gaussian functions were used for the spectral deconvolution. Such an asymmetric function is made of two half Gaussian functions which share the summit of the peak. Four parameters fully define the function, the location of the summit (E_0 , the vertical IE value), the standard deviations of the left and right half Gaussian functions σ_l and σ_r , and the scale factor δ this latter being related to the peak area ($\delta(\sigma_l + \sigma_r)/2$) and the peak height ($\delta/\sqrt{2\pi}$). This method^{2,3} has been successfully applied to analyze experimental PE spectra.⁴⁻⁶ The four fit parameters defining the PE band positions, namely the vertical IEs, were considered differently. The IE of the first band (24a MO) was set as free parameter in each PE spectrum, whilst the positions of the other three bands were defined as relative IEs referred to the first HOMO PE peak and considered equal in all the spectra, since the relative positions of the PE bands are actually constant in all the spectra. The eight left and right standard deviation free parameters, which define the peak shape of the four PE bands, were considered constant in all the spectra, namely each PE peak preserves its own shape (σ_l and σ_r values) on changing the photon energy and the angle of detection. The scale factors δ_i of the four PE bands were set as free fit parameters and specific for each PE spectrum. The global multipeak fit method¹ thus allowed the PE band relative intensities to be measured in terms of peak areas, and provided a systematic method to measure the $\beta_i(h\nu)$ parameters and the relative photoionization cross sections $\sigma_i(h\nu)$, for the valence photoionization processes of epichlorohydrin as a function of photon energy. The six PE bands at higher energies, the 20a–15a spectral components, were analysed by a simpler procedure, since all these bands share, with good approximation, the same peak shape. The whole set of the PE experimental spectra, namely recorded at all the investigated photon energies and the 0° and 54.7° detection angles, were simultaneously involved in the global multipeak fit analysis. Similarly to the first group of bands, the six peak positions were referred to the vertical IE of the HOMO band and considered as six free fit parameters, whose values are preserved in all the spectra. Here, only two standard deviation free parameters, σ_l and σ_r , were sufficient to accurately describe the peak shape of the six bands. This peak shape was considered constant, being not significantly affected by the change in photon energy and angle of detection. The six scale factors, δ_i , were defined as free fit parameters and specific for each PE spectrum. The best fit scale factors δ_i and the standard deviations σ_l and σ_r , obtained by the global fit spectral analysis, allowed us to measure the $\beta_i(h\nu)$ and $\sigma_i(h\nu)$ photoionization observables as a function of photon energy also for the high energy PE bands of epichlorohydrin. The high flexibility of the fitting package of IGOR PRO¹ allowed us to provide the bi-Gaussian function as external (user-defined) model fit function to curve fit a large set of multicomponent experimental PE spectra, simultaneously, and to define the nature, constraints, and links to freely chosen experimental data subsets of the fit parameters, according to the description given above. The large change in relative intensity of the first four PE bands, observed in

the investigated photon energy range, was fruitfully used, by means of the global multippeak fit analysis,¹ to shed more light in this congested PE spectral region.

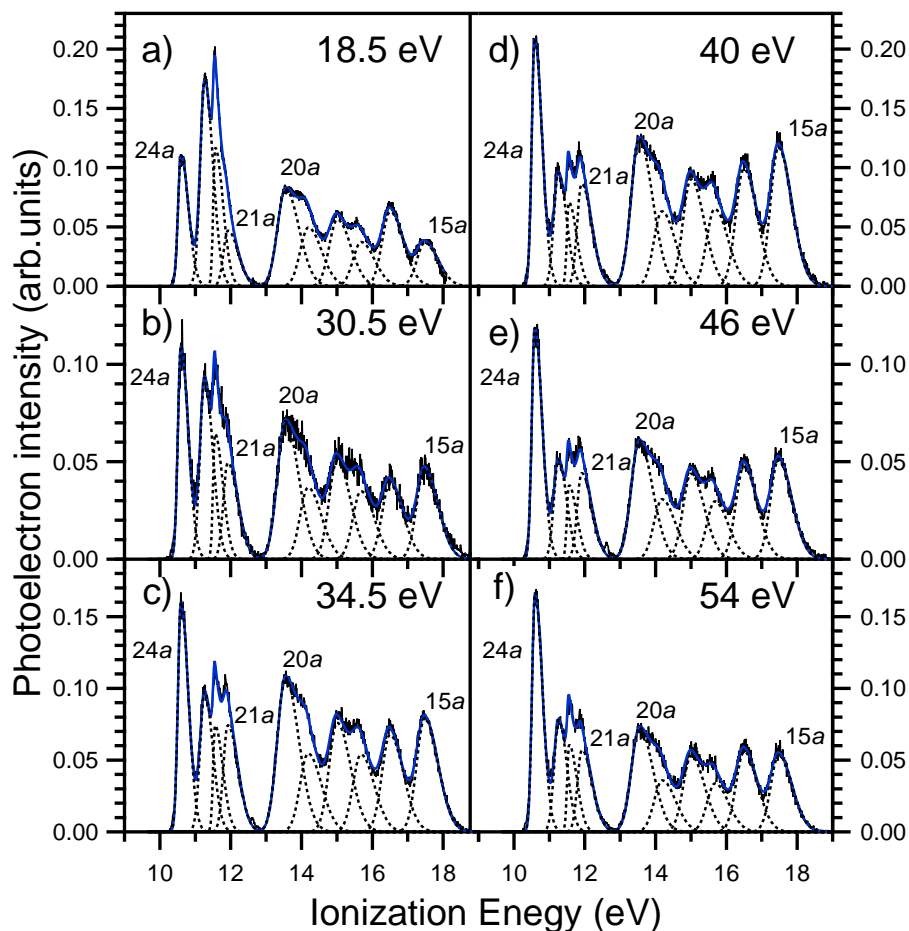


Figure S1: Outer valence PE spectra of epichlorohydrin recorded at the magic angle, $\theta = 54.7^\circ$, and at different photon energies (panels a-f). Spectral fit simulation curve (blue solid line) and bi-Gaussian fit components (dotted lines), obtained by the global multippeak fit, are shown with the experimental spectrum (solid thin line).

S2 Computational Details

The three stable conformers *cis*, *g*-I and *g*-II^{7,8} considered in this study are illustrated in Fig. S2. They differ essentially by the rotation of the CH_2Cl group around the exocyclic C-C bond with respect to the oxirane ring. The corresponding Cartesian coordinates are reported in Section S4.

The DFT and TDDFT calculations have been performed with the Tiresia program^{9,10} which employs a multicentric B-spline basis^{11,12} which is able to accurately describe both bound and continuum orbitals. The algorithms have been presented in detail in previous publications.⁹⁻¹¹ In the present case, the long-range one-center expansion has employed a linear knot sequence with range $R_{max} = 25$ au and step size $h = 0.50$ au, and maximum angular momentum $L_{max} = 14$. Short-range LCAO functions have employed R_{max} ranging from 0.8-1.2 au for H and C atoms, 1.3 au for O and 2.0 for Cl, with step size about 0.2 au, $L_{max} =$

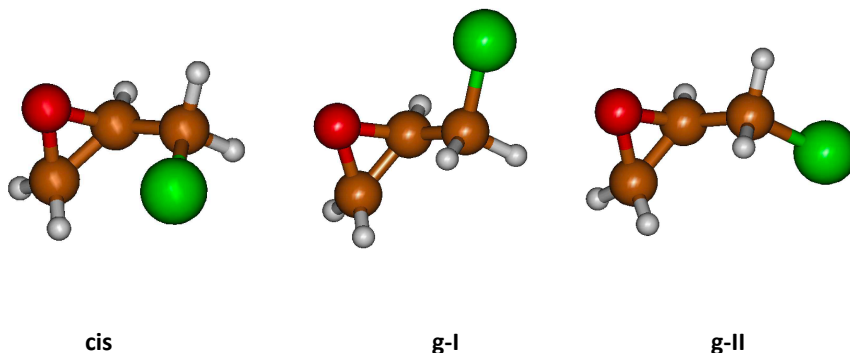


Figure S2: The three rotamers of epichlorohydrin.

1 for H and 2 for the heavier atoms. Tests have been performed to ensure that the results reported for σ and β are convergent. Initial density to define the GS Kohn-Sham Hamiltonian is obtained from a ground state calculation with the ADF program¹³ employing the STO DZP basis from the ADF database.¹⁴ Both bound and continuum orbitals are then obtained with Tiresia as eigenvectors of the KS hamiltonian, employing the LB94 exchange-correlation potential.¹⁵ In the fixed nuclei TDDFT calculations very sharp autoionization resonances appear at low energy, which are broadened by nuclear motion and are not seen in the experiment. To make comparison clearer the calculated profiles have been smoothed by a convolution with a binomial smoothing, also called gaussian smoothing with two passes.¹⁶

The ab initio EOM-CCSD calculations of the ionization energies and corresponding Dyson orbitals were carried out using Q-Chem,¹⁷ where the algorithms of Refs. 18,19 are implemented. The correlation consistent aug-cc-pVDZ basis set²⁰ of Dunning and coworkers was used. The left and right Dyson orbitals were then fed into the Tiresia code,^{9,10} that had previously been adapted to the calculation of photoionisation dynamical parameters using the EOM-CCSD Dyson orbitals.²¹

Relative energies for the three conformers have been evaluated previously⁸ as 0.00, 0.53 and 1.60 Kcal/mol for g-II, g-I and cis conformers, giving Boltzmann populations, at the experimental temperature $T=23$ °C, of 0.68, 0.28 and 0.04 respectively. An example of β profiles for the three conformers and their average is displayed in Fig. S3.

Some differences are apparent, especially for the cis conformer, whose population is, however, very small, and the average is close to the g-II profile. All σ and β profiles reported in the paper are corresponding averages over the conformers.

S3 Higher energy ionizations (deeper ionisations)

Experimental and theoretical results have also been obtained for the remaining part of the outer valence shell, 20a-15a ionizations (an expanded experimental photoelectron spectrum is presented in Ref. 8). Together with the experimental values, we present theoretical results relative only to the most accurate TDDFT continuum. For the deepest 15a ionization only initial state DFT results are evaluated, while all DFT, HF and Dyson initial orbital are presented for the other ones.

The results for the β parameter are reported in Figure S4.

Looking at the experimental results, and comparing with the four outermost ionizations, a few points

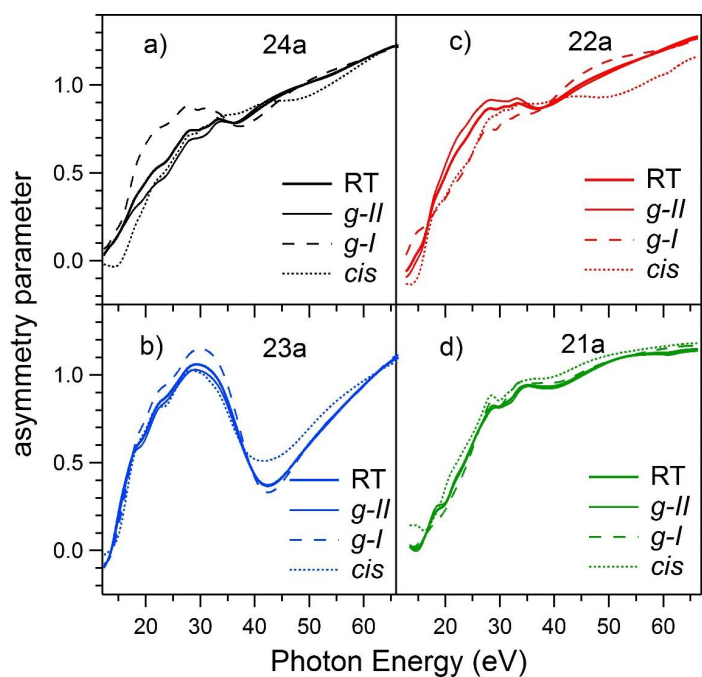


Figure S3: Epichlorohydrin. Anisotropy parameters of the stable rotamers, *g-II* (solid thin line), *g-I* (broken line), and *cis* (dotted line), for the outermost valence ionizations (panels a-d), calculated at DFT-TDDFT level. The room temperature Boltzmann average (curve RT, solid thick line) is also reported, along with the rotamers' anisotropy parameters.

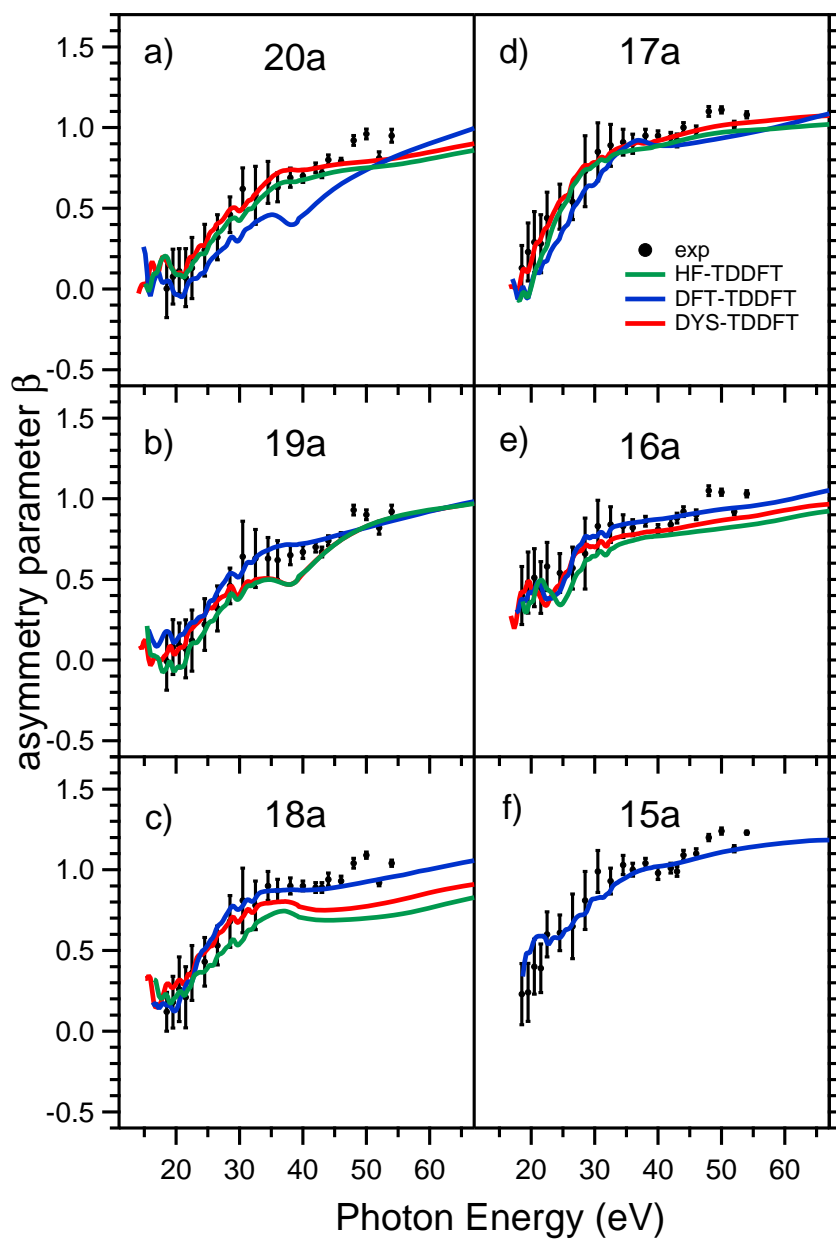


Figure S4: Epichlorohydrin. Asymmetry parameters β as a function of the photon energy for orbital 20a, 19a, 18a, 17a, 16a and 15a. Experiment versus computational results obtained using a TDDFT representation of the continuum together with Hartree-Fock (label HF-TDDFT), Density Function Theory (label DFT-TDDFT) and EOM-CCSD Dyson (label DYS-TDDFT) orbitals.

can be observed. At low energy, the β value increases smoothly, less steeply than in the outermost ones, the only exception being the 16a ionization, which displays a steep increase and a sudden flattening. Then at high energy all profiles seem to flatten around $\beta = 1$ value. Such behaviour is typical of σ orbitals of organic moieties. There are also some non conspicuous features in specific ionizations, like a kind of shallow depression around 40 eV (perhaps a sign of the CM minimum through interchannel coupling) in several channels and a dip at low energy, about 25 eV, in 16a. Generally a very satisfactory agreement with Dyson-TDDFT results is observed. Only the dip in 19a is overestimated, and too low β is displayed at high energy in 18a. More remarkable is the good general agreement of HF results with the Dyson ones, not surprising given the near validity of Koopmans theorem obtained in this region, with Dyson pretty close to HF orbitals. On the other hand, somewhat larger differences are afforded by the DFT MOs, notably in the 18a-20a channels. Similar behaviour has been observed before²² and may be due to a peculiarity of the LB94 V_{XC} potential currently employed, or a feature of the DFT approach. This would be worth further investigation.

The cross sections, reported in Fig. S5, are computed to be very similar and pretty flat, with the exception of some structure present in the 16a ionization. Also, all initial orbitals give pretty similar results, with good agreement among themselves. On the contrary, more structure is seen in the experimental results, and in particular a sudden drop of σ in the 30-40 eV region, reminiscent of the CM structure, that could be propagated through interchannel coupling effects, since negligible Cl orbital participation is expected in this region (see MO composition), despite the fact that IC is in principle included in the TDDFT description. So, agreement with the calculated values is not good, the experimental values being consistently lower above about 35eV. This behaviour largely cancels out in the BR plots displayed in Fig. S6 but still showing notable disagreements. Experimental results for 19a, 18a and 17a show a very flat BR. The agreement with the theoretical values is excellent for 18a, still good for 19a, although slightly overestimated by theory, while a low energy maximum predicted by theory is not observed in 17a, where the calculated values are also significantly overestimated. Some structure is observed in the other BRs. In the 16a channel, a low energy dip is very well matched by the theoretical results, with excellent overall agreement. Flatter BRs are theoretically predicted for the remaining 20a and 15a ionizations, while more structure in the experimental results is not reproduced, although the average value is quite well matched. As noted for the outermost ionizations, accurate reproduction of the cross sections is more difficult, as it is the accurate experimental fitting of the corresponding bands, so we cannot unambiguously attribute the observed disagreements to deficiencies in either the theoretical or experimental values, or possibly both. It is fair, however, to note that a pretty satisfactory overall description is obtained by the present EOM-CCSD Dyson-TDDFT approach.

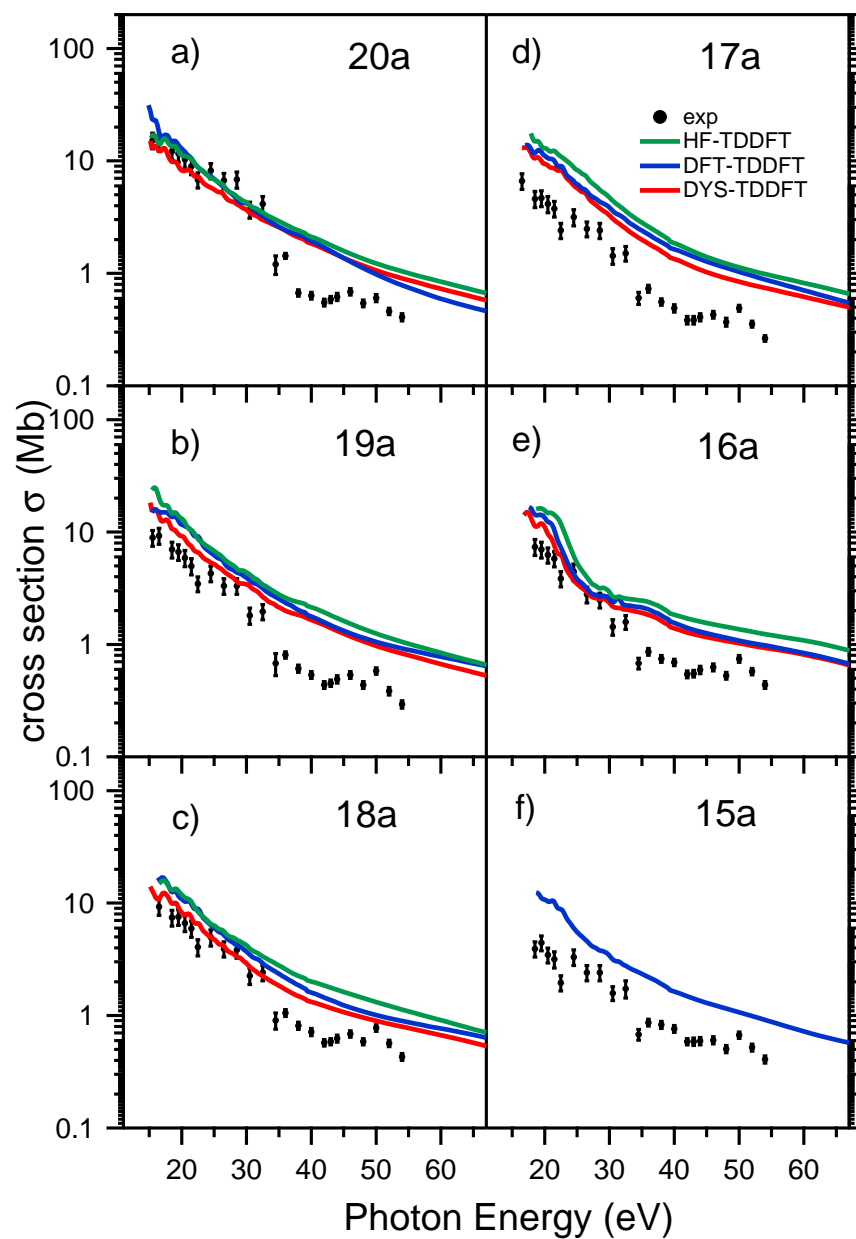


Figure S5: Epichlorohydrin. Cross-section σ as a function of the photon energy for orbitals 20a, 19a, 18a, 17a, 16a and 15a. Experiment versus computational results obtained using a TDDFT representation of the continuum together with Hartree-Fock (label HF-TDDFT), Density Function Theory (label DFT-TDDFT) and EOM-CCSD Dyson (label DYS-TDDFT) orbitals.

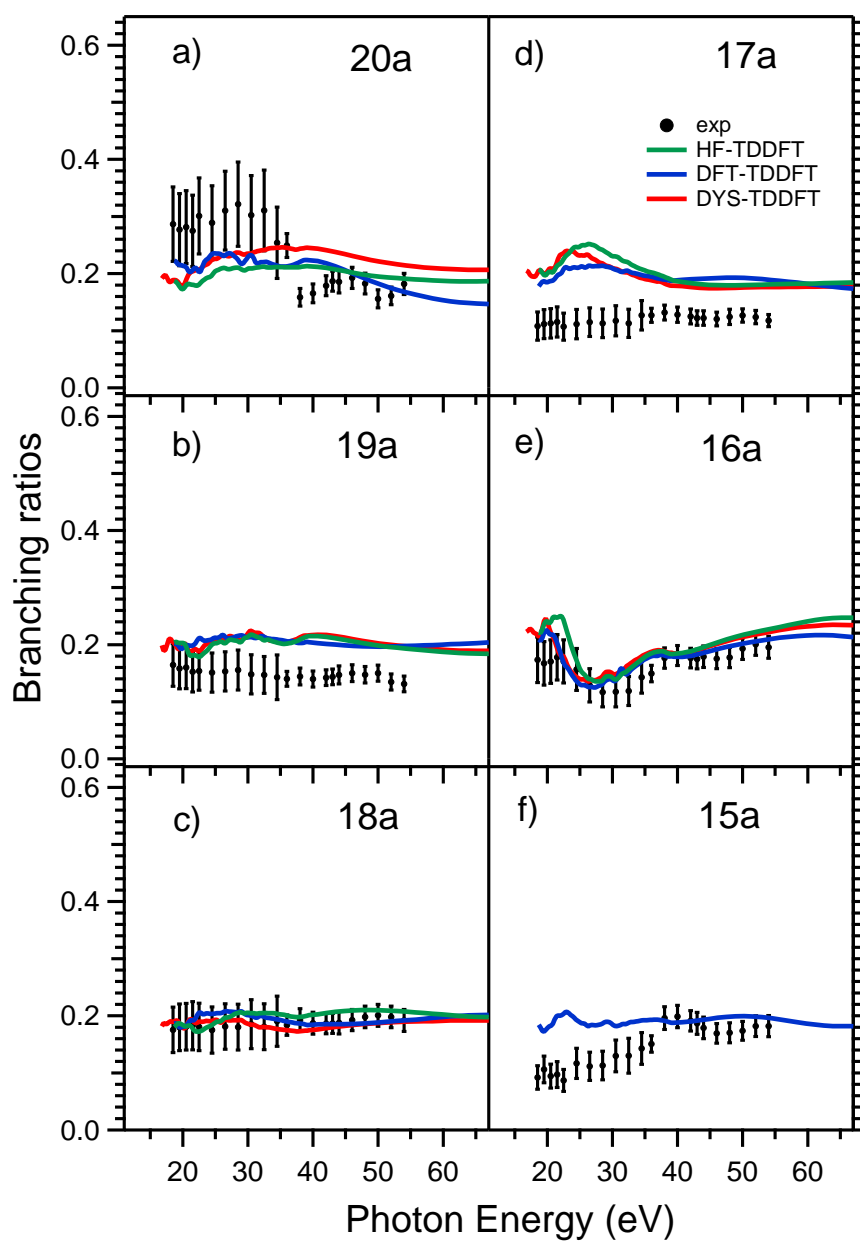


Figure S6: Epichlorohydrin. Branching ratios as a function of the photon energy for orbitals 20a, 19a, 18a, 17a, 16a and 15a. Experiment versus computational results obtained using a TDDFT representation of the continuum together with Hartree-Fock (label HF-TDDFT), Density Function Theory (label DFT-TDDFT) and EOM-CCSD Dyson (label DYS-TDDFT) orbitals.

S4 Cartesian coordinates of the three rotamers (Bohr units)

Cis

| | | | |
|----|-----------|-----------|-----------|
| C | 0.614341 | -1.086131 | -2.735336 |
| C | 1.353776 | -2.325133 | -0.396607 |
| O | 2.708330 | -0.205827 | -1.289086 |
| C | -0.008141 | -2.034237 | 2.038108 |
| Cl | -2.006889 | 0.656667 | 2.140174 |
| H | -1.044695 | 0.155827 | -2.704761 |
| H | 1.101202 | -1.974655 | -4.544451 |
| H | 2.386020 | -4.130124 | -0.528796 |
| H | 1.369614 | -1.817368 | 3.581519 |
| H | -1.181775 | -3.709235 | 2.413898 |

g-I

| | | | |
|----|-----------|-----------|-----------|
| C | -2.707614 | 0.570722 | -2.570644 |
| C | -0.590661 | -0.651584 | -1.291752 |
| O | -0.306921 | 1.750101 | -2.433162 |
| C | -0.485396 | -0.682785 | 1.493644 |
| Cl | 2.707694 | -0.570690 | 2.570566 |
| H | -4.197911 | 1.452797 | -1.427147 |
| H | -3.275343 | -0.096787 | -4.448736 |
| H | 0.412040 | -2.193443 | -2.258217 |
| H | -1.333144 | -2.417852 | 2.267780 |
| H | -1.459268 | 0.987444 | 2.261888 |

g-II

| | | | |
|----|-----------|-----------|-----------|
| C | -1.730567 | 1.567111 | -2.674188 |
| C | 0.362412 | 0.258683 | -1.464677 |
| O | 0.702434 | 2.702350 | -2.507699 |
| C | 0.552840 | 0.187234 | 1.325315 |
| Cl | -0.702291 | -2.702403 | 2.507681 |
| H | -3.191889 | 2.419594 | -1.473982 |
| H | -2.313712 | 1.013552 | -4.583473 |
| H | 1.301116 | -1.291061 | -2.481441 |
| H | 2.534850 | 0.306269 | 1.942803 |
| H | -0.517135 | 1.764267 | 2.158405 |

S5 Additional Tables and Figures

Table S1: Epichlorohydrin. HF/aug-cc-pVDZ and DFT (LB94/DZP) molecular orbital energies (eV).

| MO | cis | | g-I | | g-II | |
|-----|--------|--------|--------|--------|--------|--------|
| | HF | DFT | HF | DFT | HF | DFT |
| 24a | 11.728 | 11.927 | 11.810 | 12.061 | 11.973 | 12.142 |
| 23a | 11.945 | 12.177 | 11.891 | 12.137 | 12.054 | 12.279 |
| 22a | 12.353 | 12.567 | 12.381 | 12.461 | 12.517 | 12.571 |
| 21a | 12.898 | 13.232 | 12.843 | 13.334 | 12.816 | 13.314 |
| 20a | 14.422 | 14.470 | 14.884 | 14.721 | 14.585 | 14.738 |
| 19a | 15.075 | 15.152 | 15.211 | 15.296 | 15.102 | 15.073 |
| 18a | 15.673 | 15.662 | 15.564 | 15.669 | 16.272 | 16.118 |
| 17a | 17.442 | 16.649 | 17.116 | 16.553 | 16.871 | 16.362 |
| 16a | 18.095 | 17.224 | 18.394 | 17.441 | 18.340 | 17.380 |

Table S2: Mulliken atomic 2p (and Cl 3p) populations of the HF MO. C1 is the -CH₂ carbon in the ring, C2 is the CH carbon and C3 is the carbon bound to the Cl atom. Other populations, with the exception of H 1s, are very small and therefore omitted.

| g-II | | | | | | | | | | | |
|------|------|-------|-------|-------|-------|-------|-------|-------|-------|-------|-------|
| Atom | Orb. | MO | | | | | | | | | |
| | | 15 | 16 | 17 | 18 | 19 | 20 | 21 | 22 | 23 | 24 |
| C 1 | p | 0.263 | 0.340 | 0.054 | 0.154 | 0.325 | 0.109 | 0.127 | 0.484 | 0.010 | 0.134 |
| C 2 | p | 0.295 | 0.284 | 0.070 | 0.088 | 0.321 | 0.098 | 0.093 | 0.415 | 0.089 | 0.105 |
| O | p | 0.422 | 0.441 | 0.201 | 0.635 | 0.006 | 0.536 | 1.150 | 0.377 | 0.281 | 0.097 |
| C 3 | p | 0.223 | 0.419 | 0.744 | 0.374 | 0.336 | 0.314 | 0.016 | 0.028 | 0.081 | 0.103 |
| Cl | p | 0.038 | 0.057 | 0.226 | 0.355 | 0.164 | 0.586 | 0.322 | 0.539 | 1.428 | 1.281 |
| g-I | | | | | | | | | | | |
| C 1 | p | 0.261 | 0.364 | 0.199 | 0.168 | 0.138 | 0.227 | 0.140 | 0.393 | 0.000 | 0.169 |
| C 2 | p | 0.295 | 0.295 | 0.107 | 0.035 | 0.232 | 0.238 | 0.111 | 0.366 | 0.009 | 0.195 |
| O | p | 0.472 | 0.413 | 0.207 | 0.271 | 0.479 | 0.406 | 1.033 | 0.638 | 0.044 | 0.160 |
| C 3 | p | 0.238 | 0.402 | 0.647 | 0.581 | 0.419 | 0.174 | 0.025 | 0.050 | 0.080 | 0.065 |
| Cl | p | 0.037 | 0.048 | 0.161 | 0.522 | 0.371 | 0.117 | 0.421 | 0.263 | 1.702 | 1.340 |
| cis | | | | | | | | | | | |
| C 1 | p | 0.250 | 0.335 | 0.017 | 0.217 | 0.240 | 0.162 | 0.141 | 0.432 | 0.053 | 0.125 |
| C 2 | p | 0.293 | 0.325 | 0.101 | 0.088 | 0.152 | 0.224 | 0.115 | 0.365 | 0.113 | 0.094 |
| O | p | 0.460 | 0.453 | 0.097 | 0.196 | 0.849 | 0.137 | 0.923 | 0.487 | 0.294 | 0.221 |
| C 3 | p | 0.273 | 0.284 | 0.887 | 0.522 | 0.293 | 0.318 | 0.018 | 0.021 | 0.082 | 0.098 |
| Cl | p | 0.056 | 0.085 | 0.156 | 0.459 | 0.089 | 0.542 | 0.608 | 0.499 | 1.265 | 1.229 |

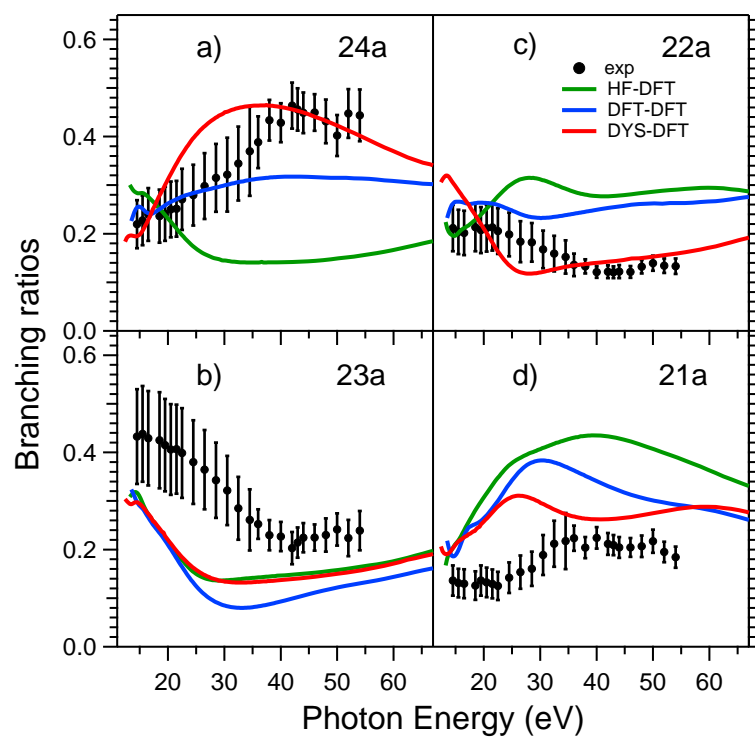


Figure S7: Epichlorohydrin. Branching ratios for orbitals 24, 23, 22 and 21 as a function of the photon energy. Experiment versus computational results obtained using a DFT representation of the continuum together with Hartree-Fock (HF-DFT), Density Function Theory (DFT-DFT) and EOM-CCSD Dyson (DYS-DFT) orbitals

S6 Comparison between experimental and theoretical observables

The sample experimentally investigated is modeled as a gaseous mixture of the three stable rotamers of epichlorohydrin, present with their Boltzmann relative weights at the experimental temperature, namely g-II (0.68), g-I (0.28), and cis (0.04). The theoretical calculations provide the photoionization observables for each of the three rotamers, thus allowing to derive the average value of the calculated observable, which is compared to the experimental one.

Partial cross sections In addition to what described in the main text, only additional complementary details are given here. The experimental partial cross sections for the 20a-15a ionization channels are compared to the corresponding calculated values in Figure S5 using the same conversion factor derived for the comparison of the 24a-21a channels shown in Fig. 4 and Fig. 5. The branching ratio of the 20a-15a ionizations reported in Figure S6 is given as the ratio between the PE peak area of the specific ionization and the sum of the corresponding areas of the 20a-15a ionizations.

Asymmetry parameters All the measured experimental asymmetry parameters β_{ex}^j , in Fig. 2, Fig. 3, and Fig. S4, are compared to the corresponding average calculated value β_{av}^j , which is derived from the following formula,

$$\beta_{i,\text{av}} = \frac{\sum_j p_j \sigma_{i,j} \beta_{i,j}}{\sum_j p_j \sigma_{i,j}} \quad (\text{S1})$$

where p_j is the Boltzmann relative weight of the j -th rotamer (with $j = \text{g-II}, \text{g-I}, \text{and cis}$), and i is referring to the i -th ionization channel. The formula for the average is derived in the next section.

S7 Derivation of β_{av} over conformers

Let us consider a statistical mixture of N conformers with populations (Boltzmann weights)

$$p_j, \quad \sum_j p_j = 1 \quad j = 1, \dots, N \quad (\text{S2})$$

Omitting the subscript i for the ionisation channel for ease of notation, the differential cross section for each conformer is given by

$$\frac{d\sigma_j}{d\theta} = \frac{\sigma_j}{4\pi} [1 + \beta_j P_2(\cos \theta)] \quad j = 1, \dots, N \quad (\text{S3})$$

which is valid at all angles. The total differential cross section is then given by the weighted sum of the individual terms

$$\frac{d\sigma_{\text{av}}}{d\theta} = \sum_j p_j \frac{d\sigma_j}{d\theta} . \quad (\text{S4})$$

Substituting eq. (S3) in the right hand side one obtains

$$\begin{aligned}
\frac{d\sigma_{\text{av}}}{d\theta} &= \sum_j p_j \frac{\sigma_j}{4\pi} [1 + \beta_j P_2(\cos \theta)] \\
&= \frac{1}{4\pi} \left(\sum_j p_j \sigma_j + \sum_j p_j \sigma_j \beta_j P_2(\cos \theta) \right) \\
&= \frac{1}{4\pi} \left\{ \sum_j p_j \sigma_j + \left(\sum_j p_j \sigma_j \beta_j \right) P_2(\cos \theta) \right\} \\
&= \frac{1}{4\pi} (\sigma_{\text{av}} + B_{\text{av}} P_2(\cos \theta)) \\
&= \frac{\sigma_{\text{av}}}{4\pi} [1 + \beta_{\text{av}} P_2(\cos \theta)] \tag{S5}
\end{aligned}$$

with

$$\sigma_{\text{av}} = \sum_j p_j \sigma_j \quad \beta_{\text{av}} = \frac{B_{\text{av}}}{\sigma_{\text{av}}} = \frac{\sum_j p_j \sigma_j \beta_j}{\sum_j p_j \sigma_j} \tag{S6}$$

which is still valid at all angles. Thus, if one measures the average differential cross section at two angles (e.g., zero and the magic angle), one can extract from this the value of β_{av} , obtained by averaging the individual β_j weighted as in eq (S6).

References

- [1] Global Multippeak Fitting Package implemented in the IGOR PRO data analysis program (WaveMetrics, Inc.).
- [2] T. Yu and H. Peng, *BMC Bioinformatics*, 2010, **11**, 559.
- [3] T. S. Buys and K. De Clerk, *Anal. Chem.*, 1972, **44**, 1273–1275.
- [4] A. Boccia, A. G. Marrani, S. Stranges, R. Zanoni, M. Alagia, M. Cossi and M. F. Iozzi, *J. Chem. Phys.*, 2008, **128**, 154315.
- [5] D. L. Lichtenberger and A. S. Copenhaver, *Journal of Electron Spectroscopy and Related Phenomena*, 1990, **50**, 335–352.
- [6] D. L. Lichtenberger and R. F. Fenske, *J. Am. Chem. Soc.*, 1976, **98**, 50–63.
- [7] M. C. Tam and T. D. Crawford, *J. Phys. Chem. A*, 2006, **110**, 2290–2298.
- [8] S. Stranges, M. Alagia, P. Decleva, M. Stener, G. Fronzoni, D. Toffoli, M. Speranza, D. Catone, S. Turchini, T. Prosperi, N. Zema, G. Contini and Y. Keheyan, *Phys. Chem. Chem. Phys.*, 2011, **13**, 12517–12528.
- [9] P. Decleva, M. Stener and D. Toffoli, *Molecules*, 2022, **27**, 2026.
- [10] D. Toffoli, S. Coriani, M. Stener and P. Decleva, *Comp. Phys. Comm.*, 2024, **297**, 109038.
- [11] D. Toffoli, M. Stener, G. Fronzoni and P. Decleva, *Chem. Phys.*, 2002, **276**, 25–43.
- [12] H. Bachau, E. Cormier, P. Decleva, J. E. Hansen and F. Martín, *Rep. Prog. Phys.*, 2001, **64**, 1815–1943.
- [13] G. te Velde, F. M. Bickelhaupt, E. J. Baerends, C. Fonseca Guerra, S. J. A. van Gisbergen, J. G. Snijders and T. Ziegler, *J. Comput. Chem.*, 2001, **22**, 931–967.
- [14] E. Van Lenthe and E. J. Baerends, *J. Comput. Chem.*, 2003, **24**, 1142–1156.
- [15] R. van Leeuwen and E. J. Baerends, *Phys. Rev. A*, 1994, **49**, 2421–2431.
- [16] P. Marchand and L. Marmet, *Rev. Sci. Instrum.*, 1983, **54**, 1034–41.
- [17] E. Epifanovsky, A. T. B. Gilbert, X. Feng, J. Lee, Y. Mao, N. Mardirossian, P. Pokhilko, A. F. White, M. P. Coons, A. L. Dempwolff, Z. Gan, D. Hait, P. R. Horn, L. D. Jacobson, I. Kaliman, J. Kussmann, A. W. Lange, K. U. Lao, D. S. Levine, J. Liu, S. C. McKenzie, A. F. Morrison, K. D. Nanda, F. Plasser, D. R. Rehn, M. L. Vidal, Z.-Q. You, Y. Zhu, B. Alam, B. J. Albrecht, A. Aldossary, E. Alguire, J. H. Andersen, V. Athavale, D. Barton, K. Begam, A. Behn, N. Bellonzi, Y. A. Bernard, E. J. Berquist, H. G. A. Burton, A. Carreras, K. Carter-Fenk, R. Chakraborty, A. D. Chien, K. D. Closser, V. Cofer-Shabica, S. Dasgupta, M. de Wergifosse, J. Deng, M. Diedenhofen, H. Do, S. Ehlert, P.-T. Fang, S. Fatehi, Q. Feng, T. Friedhoff, J. Gayvert, Q. Ge, G. Gidofalvi, M. Goldey, J. Gomes, C. E. González-Espinoza, S. Gulania, A. O. Gunina, M. W. D. Hanson-Heine, P. H. P. Harbach, A. Hauser, M. F. Herbst, M. Hernández Vera, M. Hodecker, Z. C. Holden, S. Houck, X. Huang, K. Hui, B. C. Huynh, M. Ivanov, A. Jász, H. Ji, H. Jiang, B. Kaduk, S. Kähler, K. Khistyayev, J. Kim, G. Kis, P. Klunzinger, Z. Koczor-Benda, J. H. Koh, D. Kosenkov, L. Koulias, T. Kowalczyk, C. M. Krauter, K. Kue, A. Kunitsa, T. Kus, I. Ladjánszki, A. Landau, K. V. Lawler, D. Lefrancois, S. Lehtola, R. R. Li, Y.-P. Li, J. Liang, M. Liebenthal, H.-H. Lin, Y.-S. Lin, F. Liu, K.-Y. Liu, M. Loipersberger, A. Luenser, A. Manjanath, P. Manohar, E. Mansoor, S. F. Manzer, S.-P. Mao, A. V. Marenich, T. Markovich, S. Mason, S. A. Maurer, P. F. McLaughlin, M. F. S. J. Menger, J.-M. Mewes, S. A. Mewes, P. Morgante, J. W. Mullinax, K. J. Oosterbaan, G. Paran, A. C. Paul, S. K. Paul, F. Pavošević, Z. Pei, S. Prager, E. I. Proynov,

Á. Rák, E. Ramos-Cordoba, B. Rana, A. E. Rask, A. Rettig, R. M. Richard, F. Rob, E. Rossomme, T. Scheele, M. Scheurer, M. Schneider, N. Sergueev, S. M. Sharada, W. Skomorowski, D. W. Small, C. J. Stein, Y.-C. Su, E. J. Sundstrom, Z. Tao, J. Thirman, G. J. Tornai, T. Tsuchimochi, N. M. Tubman, S. P. Veccham, O. Vydrov, J. Wenzel, J. Witte, A. Yamada, K. Yao, S. Yeganeh, S. R. Yost, A. Zech, I. Y. Zhang, X. Zhang, Y. Zhang, D. Zuev, A. Aspuru-Guzik, A. T. Bell, N. A. Besley, K. B. Bravaya, B. R. Brooks, D. Casanova, J.-D. Chai, S. Coriani, C. J. Cramer, G. Cserey, A. E. DePrince, R. A. DiStasio, A. Dreuw, B. D. Dunietz, T. R. Furlani, W. A. Goddard, S. Hammes-Schiffer, T. Head-Gordon, W. J. Hehre, C.-P. Hsu, T.-C. Jagau, Y. Jung, A. Klamt, J. Kong, D. S. Lambrecht, W. Liang, N. J. Mayhall, C. W. McCurdy, J. B. Neaton, C. Ochsenfeld, J. A. Parkhill, R. Peverati, V. A. Rassolov, Y. Shao, L. V. Slipchenko, T. Stauch, R. P. Steele, J. E. Subotnik, A. J. W. Thom, A. Tkatchenko, D. G. Truhlar, T. Van Voorhis, T. A. Wesolowski, K. B. Whaley, H. L. Woodcock, P. M. Zimmerman, S. Faraji, P. M. W. Gill, M. Head-Gordon, J. M. Herbert and A. I. Krylov, *J. Chem. Phys.*, 2021, **155**, 084801.

- [18] C. M. Oana and A. I. Krylov, *J. Chem. Phys.*, 2007, **127**, 234106.
- [19] C. M. Oana and A. I. Krylov, *J. Chem. Phys.*, 2009, **131**, 124114.
- [20] D. E. Woon and T. H. Dunning Jr., *J. Chem. Phys.*, 1994, **100**, 2975.
- [21] T. Moitra, A. Ponzi, H. Koch, S. Coriani and P. Decleva, *J. Phys. Chem. Lett.*, 2020, **11**, 5330–5337.
- [22] T. Moitra, S. Coriani and P. Decleva, *J. Chem. Theory Comput.*, 2021, **17**, 5064–5079.